CADM1 Interacts with Tiam1 and Promotes Invasive Phenotype of Human T-cell Leukemia Virus Type I-transformed Cells and Adult T-cell Leukemia Cells*[S]

Mari Masuda,[a,b1] Tomoko Maruyama,[b,c] Tsutomu Ohta,[a] Akihiko Ito,[c] Tomayoshi Hayashi,[d] Kunihiko Tsukasaki,[e] Shimeru Kamihira,[f] Shoji Yamaoka,[g] Hiroo Hoshino,[h] Teruhiko Yoshida,[a] Toshiki Watanabe,[i] Eric J. Stanbridge,[j] and Yoshinori Murakami[b,c2]

From the [a]Genetics Division and [b]Tumor Suppression and Functional Genomics Project, National Cancer Center Research Institute, Tokyo 104-0045, Japan, the [c]Division of Molecular Pathology, Department of Cancer Biology, Institute of Medical Science, and the [i]Laboratory of Tumor Cell Biology, Department of Medical Genome Sciences, Graduate School of Frontier Sciences, University of Tokyo, Tokyo 108-8639, Japan, the [d]Department of Pathology, [e]Department of Molecular Medicine and Hematology, and [f]Department of Laboratory Medicine, Nagasaki University Graduate School of Biomedical Sciences, Nagasaki 852-8523, Japan, the [g]Department of Molecular Virology, Graduate School of Medicine, Tokyo Medical and Dental University, Tokyo 113-8510, Japan, the [h]Department of Virology and Preventive Medicine, Gunma University Graduate School of Medicine, Maebashi 371-8511, Japan, and the[j]Department of Microbiology and Molecular Genetics, College of Medicine, University of California, Irvine, California 92697

CADM1 encodes a multifunctional immunoglobulin-like cell adhesion molecule whose cytoplasmic domain contains a type II PSD95/Dlg/ZO-1 (PDZ)-binding motif (BM) for associating with other intracellular proteins. Although CADM1 lacks expression in T lymphocytes of healthy individuals, it is overexpressed in adult T-cell leukemia-lymphoma (ATL) cells. It has been suggested that the expression of CADM1 protein promotes infiltration of leukemic cells into various organs and tissues, which is one of the frequent clinical manifestations of ATL. Amino acid sequence alignment revealed that Tiam1 (T-lymphoma invasion and metastasis 1), a Rac-specific guanine nucleotide exchange factor, has a type II PDZ domain similar to those of membrane-associated guanylate kinase homologs (MAGUKs) that are known to bind to the PDZ-BM of CADM1. In this study, we demonstrated that the cytoplasmic domain of CADM1 directly interacted with the PDZ domain of Tiam1 and induced formation of lamellipodia through Rac activation in HTLV-I-transformed cell lines as well as ATL cell lines. Our results indicate that Tiam1 integrates signals from CADM1 to regulate the actin cytoskeleton through Rac activation, which may lead to tissue infiltration of leukemic cells in ATL patients.

CADM1 is the recently unified nomenclature for TSLC1 (tumor suppressor in non-small cell lung cancer 1) (1), which had a variety of different names, including IGSF4A (2), RA175 (3), SgIGSF (4), SynCAM1 (5), and Necl-2 (6) due to its previously reported multiple functions. CADM1 encodes an immunoglobulin-like cell adhesion molecule with three immunoglobulin loops. The ectodomain of CADM1 mediates intercellular adhesion through homophilic or heterophilic trans-interaction between neighboring cells (7). Despite being a tumor suppressor in various carcinomas, recent DNA microarray analysis of primary adult T-cell leukemia/lymphoma (ATL)[3] cells from acute type ATL patients revealed that CADM1 was up-regulated over 30-fold in those patients through an as yet unknown mechanism (8). ATL is a neoplastic disease of CD4-positive T lymphocytes that is etiologically associated with human T-cell leukemia virus type I (HTLV-I) (9). ATL develops in 3–5% of HTLV-I-infected individuals after an extended latent period of ~40–60 years (10), yet it remains an aggressive disease with poor prognosis and a median survival time of 11–13 months reported even in patients treated with the most effective first line combination chemotherapy (11). ATL is well known for its propensity of infiltrating leukemic cells into various organs and tissues, such as the skin, lungs, liver, gastrointestinal tract, central nervous system, lymph nodes, and bone (12). Previous studies reported that various cell adhesion molecules, cytokines, chemokines, and chemokine receptors are implicated in the process of ATL cell infiltration (13). Because cell adhesion is a critical step in tumor cell invasion, it has been proposed that over-

[3] The abbreviations used are: ATL, adult T-cell leukemia/lymphoma; HTLV-I, human T-cell leukemia virus type I; GEF, guanine nucleotide exchange factor; PDZ, PSD95/Dlg/ZO-1; DH, Dbl homology; GST, glutathione S-transferase; MAGUK, membrane-associated guanylate kinase homolog; BM, binding motif; Dox, doxycycline; mAb, monoclonal antibody; pAb, polyclonal antibody; HEK, human embryonic kidney; NHDF, normal human dermal fibroblast(s); HMVEC, human adult dermal microvascular endothelial cell(s); BisTris, 2-[bis(2-hydroxyethyl)amino]-2-(hydroxymethyl)propane-1,3-diol.

expression of CADM1 accelerates the tissue infiltration of ATL cells (8).

The cytoplasmic domain of CADM1 contains two conserved protein-interaction modules (1). One is the submembranous protein 4.1-binding motif (protein 4.1-BM) in which members of the protein 4.1 family bind and link CADM1 to the actin cytoskeleton (14). The other is the C-terminal EYFI sequence called the type II PDZ-binding motif (PDZ-BM), in which membrane-associated guanylate kinase homologs (MAGUKs) interact through their PDZ (PSD-95, Discs large and ZO-1) domains (6, 15). PDZ domains are composed of ~90 amino acids and bind to the C-terminal PDZ-binding motif of target protein. Type I, II, and III PDZ domains recognize $E(S/T)X(V/I)$, $\Phi X\Phi$, and $XDXV$, respectively, where X is any amino acid and Φ is a hydrophobic amino acid residue (16, 17). Proteins harboring PDZ-BM interact with PDZ domain-containing proteins and induce various cellular functions. One well known example is the Tax oncoprotein encoded by HTLV-I, a key player of ATL leukemogenesis, which has type I PDZ-BM, ETEV, at the C terminus. Tax exerts transforming activities by binding with several intracellular PDZ domain-containing proteins (18, 19), which are believed to be involved in ATL leukemogenesis. Bioinformatic analysis of the amino acid sequence revealed that Tiam1 (T-lymphoma invasion and metastasis 1) has a type II PDZ domain that shares significant similarities with those of MAGUKs. *Tiam1* was originally identified as an invasion- and metastasis-inducing gene in murine T-lymphoma cells that encodes a guanine nucleotide exchange factor (GEF) specific for Rac, a member of the Rho GTPases (20, 21). Rho GTPases, including Rho, Rac, and Cdc42, act as molecular switches by cycling between active (GTP-bound) and inactive (GDP-bound) states to regulate actin dynamics that are involved in diverse cellular responses, including cell adhesion and motility (22). The activation of Rho GTPases is mediated by specific GEFs that catalyze the exchange of GDP for GTP. In their active state, Rho GTPases bind to their effectors with high affinity, thereby eliciting downstream responses (22). It has been well documented that reorganization of the actin cytoskeleton by Rho GTPases is the primary mechanism of cell motility and is essential for most types of cell migration. Among the Rho GTPases, Rac has long been known to induce the formation of actin-rich membrane ruffles or lamellipodia at the leading edge of motile cells that are required for forward movement of migratory cells (22–24). Overexpression of Tiam1 is known to increase invasion of T lymphoma cells into a fibroblast monolayer (21) as well as to induce formation of lamellipodia and cell spreading through activation of Rac. There is a growing body of evidence indicating that the interaction between GEFs and other proteins through PDZ motifs is a general mechanism for controlling the exchange activity of GEFs (25). No scaffold protein or integral membrane protein has as yet been reported to associate with the PDZ domain of Tiam1, although this seems highly probable. We hypothesized, therefore, that in addition to its role as an anchor of the actin cytoskeleton to the cell membrane through protein 4.1, CADM1 is able to recruit Rac-specific GEF Tiam1 to the cell membrane and induce reorganization of the cortical actin in ATL cells, thereby rendering ATL cells motile. This scenario could explain the invasive nature of ATL cells overexpressing CADM1.

In the present study, we have demonstrated that the cytoplasmic domain of CADM1 directly associates with Tiam1 through the PDZ domain of Tiam1 and induces formation of lamellipodia through Rac activation in both HTLV-I-transformed cell lines and ATL cell lines. This interaction between CADM1 and Tiam1, therefore, could play a role in infiltration of leukemic cells into various organs and tissues in ATL patients.

EXPERIMENTAL PROCEDURES

Cells—Jurkat, Molt-4, CCRF-CEM, T-all, and CEM/C2 cell lines derived from acute lymphoblastic T-cell leukemia patients and H9 and Hut78 derived from cutaneous T-cell lymphoma were obtained from the American Type Culture Collection (ATCC). The Jurkat Tet-Off cell line was purchased from Takara Bio. HTLV-I-transformed cell lines used in this study, MT-2, MT-4, C91/PL, and C8166–45, were supplied from the National Institutes of Health AIDS Research and Reference Reagent Program. ATL-1K, TL-Om1, and ATL-43Tb(−) cell lines were leukemic T-cell lines derived from ATL patients and provided by Masanao Miwa (Nagahama Institute of Bio-science and Technology, Nagahama, Japan), Kazuo Sugamura (Tohoku University, Sendai, Japan), and Michiyuki Maeda (Kyoto University, Kyoto, Japan), respectively. The ATL-3I cell line was described previously (26). All T cell lines described above were maintained in RPMI medium (Sigma) supplemented with 10% Tet system-approved fetal bovine serum (Takara Bio), 100 units/ml penicillin, and 100 μg/ml streptomycin (Invitrogen). Mouse NIH3T3 fibroblasts and human embryonic kidney (HEK) 293 cells were from the ATCC and grown in Dulbecco's modified Eagle's medium supplemented with 10% fetal bovine serum (Sigma), 100 units/ml penicillin, and 100 μg/ml streptomycin. Normal human dermal fibroblasts (NHDF) and human adult dermal microvascular endothelial cells (HMVEC) were purchased from Lonza Walkersville Inc. and maintained in culture media specified by the manufacturer's instructions.

Antibodies and Reagents—Mouse monoclonal antibodies (mAbs) specific to V5 (R960-25), CD44 (C26), Talin (8D4), and α-tubulin (sc-8035) were obtained from Invitrogen, BD Biosciences, Sigma, and Santa Cruz Biotechnology, Inc. (Santa Cruz, CA), respectively. CADM1 antibodies used in this study were rabbit polyclonal antibodies (pAbs) against the cytoplasmic domain, CC2 (7), and number 6 (27); a rabbit pAb against the ectodomain, EC (28); and a chicken mAb against the ectodomain, 3E1 (29). A rabbit pAb to Tiam1 (C16) was purchased from Santa Cruz Biotechnology, Inc. Secondary antibodies used for immunoblot analysis were from GE Healthcare. For immunofluorescent staining, all fluorophore-conjugated secondary antibodies were obtained from Jackson Immunoresearch Laboratories. Alexa Fluor 568-phalloidin or Alexa Fluor 633-phalloidin (Invitrogen) was used to visualize the actin cytoskeleton.

Construction of Expression Vectors—Full-length human Tiam1 cDNA was generated from adult human brain poly(A) RNA (Takara Bio) by RT-PCR using the Superscript first strand synthesis system (Invitrogen) and the Expand high fidelity PCR system

(Roche Applied Science) and cloned into either a pcDNA3.1hygro(+) vector (Invitrogen) for expressing Tiam1 (pcDNA3.1/Tiam1) or a pcDNA3.1/V5-HIS-TOPO vector (Invitrogen) for expressing Tiam1 tagged with V5 (pcDNA3.1/Tiam1-V5). The pcDNA3.1/Tiam1-V5 was used as a template to create truncated Tiam-V5 constructs by PCR. For construction of C1199-V5 and C580-V5 mutants, the N-terminal 392 and 1011 amino acid residues were removed, respectively (Fig. 2C). The truncated mutant C1199ΔPDZ-V5 was designed to remove 146 amino acids (residues 817–962) encompassing the PDZ domain from the C1199 mutant (Fig. 2C). In generating pcDNA3.1/PDZ-V5, the PDZ fragment (amino acids 817–972) of Tiam1 was amplified by PCR and subcloned into a pcDNA3.1/V5-HIS-TOPO vector. Construction of pTRE2/CADM1 expressing full-length CADM1 and pTRE2/ΔC-HA expressing CADM1 lacking its cytoplasmic tail was described previously (30). Nucleotide sequences of all PCR-amplified fragments were confirmed by sequencing. A plasmid encoding the human dominant negative mutant of Rac1, Rac1(T17N), was obtained from Upstate, and the EcoRI-PmeI fragment containing the coding region of Rac1(T17N) was subcloned into a pEGFP-N3 vector at the EcoRI and SmaI sites (Takara Bio). The constructs for the N-terminal glutathione *S*-transferase (GST)-tagged cytoplasmic domain of CADM1 (GST-CADM1-C) and the truncated mutant lacking the C-terminal 3 amino acids (GST-CADM1-CΔ3) were also described previously (15).

Transfection—To obtain Jurkat Tet-Off cell clones expressing full-length CADM1 or the mutant lacking the cytoplasmic domain of CADM1, cells were transfected with pTRE2/CADM1 or pTRE2/ΔC-HA using Fugene 6 (Roche Applied Science) and selected in a medium containing 300 μg/ml hygromycin (Invitrogen). Transient transfection of HEK293 cells and T cell lines with plasmids were also performed with Fugene 6.

RNA Interference—Target sequences for small interfering RNA were as follows: for human CADM1, 5′-CTGGCCCTA-TTTAGATGATAA-3′ (CADM1 siRNA 1) and 5′-AACGAA-AGACGTGACAGTGAT-3′ (CADM1 siRNA 2); for human Tiam1, 5′-AACATGTAGAGCACGAGTTTT-3′ (Tiam1 siRNA 1) and 5′-CGGCGAGCTTTAAGAAGAA-3′ (Tiam1 siRNA 2). The RNA duplexes (Qiagen) were introduced into cells by electroporation using a Microporator (Digital Bio Technology) according to the manufacturer's instruction. AllStars negative control siRNA (Qiagen) was used as the control.

Cell Adhesion Assay—Cell adhesion assays were performed with a Vybrant cell adhesion assay kit (Invitrogen) according to the manufacturer's protocol. Briefly, cells labeled with calcein AM were co-cultured on NHDF monolayers for 2 h. After removing the nonadherent cells, the absorbance at 494 nm was measured with a multilabel counter Wallac 1420 ARVOsx (PerkinElmer Life Sciences).

GST Pull-down Assay—GST-CADM1 fusion proteins expressed in *Escherichia coli* were purified with glutathione Sepharose 4B (GE Healthcare). [³⁵S]Methionine-labeled full-length Tiam1 and deletion mutants were synthesized in reticulocytes using a TNT T7 Quick Coupled transcription/translation system (Promega). A GST pull-down assay was performed as described previously (14).

Immunoblot Analysis and Immunoprecipitation—Preparation of cell lysates and immunoblot analysis were described previously (7). A rabbit anti-CADM1 pAb, CC2, was used for detecting CADM1 by immunoblot analysis. For immunoprecipitation, cell lysates containing 500 μg of protein were first precleared by incubation with protein A-Sepharose or protein G-Sepharose (GE Healthcare) for 3 h at 4 °C. The precleared lysates were then incubated with a rabbit anti-CADM1 pAb, EC1, or a mouse anti-V5 mAb overnight at 4 °C. A rabbit IgG or mouse IgG was used as a negative control. The protein-antibody conjugates were precipitated with protein A-Sepharose or protein G-Sepharose for 1 h at 4 °C. Immunoprecipitates were rinsed three times with the lysis buffer, fractionated either in a 4–12% gradient Nupage gel (Invitrogen) or a 3–5% Tris acetate Nupage gel (Invitrogen), and then immunoblotted.

Immunocytochemistry and Confocal Microscopy—Immunostaining and confocal microscopy with either a Carl Zeiss LSM510 or Bio-Rad Radiance 2000 laser confocal scanning system were described previously (7, 30).

Human Samples and Histological Examination—ATL patients underwent excisional biopsies of lymph nodes at Nagasaki University Hospital from 1998 to 2006. The diagnosis of ATL was based on clinical features and hematological findings, including histologically proven mature T-cell leukemia/lymphoma and serum anti-HTLV-I antibodies. Immunohistochemical analyses of formalin-fixed and paraffin-embedded tissue sections were performed as described previously (31, 32).

RESULTS

Expression of CADM1 and Tiam1 in HTLV-I-transformed Cell Lines and ATL Cell Lines—We first examined localization of CADM1 in HTLV-I-transformed cell lines and ATL cell lines. When cultured in media, these cells tend to grow in aggregates as observed in HTLV-I-transformed MT-2 cells (Fig. 1A). CADM1 was concentrated at cell-cell contact sites (Fig. 1A), indicating that homophilic *trans*-interaction of CADM1 may have promoted the formation of these cell aggregates. In epithelia, homophilic *trans*-interaction of CADM1 mediates adhesion of apposing cells (30), and the PDZ-BM of CADM1 associates with MAGUKs, such as MPP3 (15), Pals2 (6), and CASK (5). It has been suggested that the interaction of CADM1 and MAGUKs plays a role in maintaining epithelial morphology (33). In an attempt to elucidate the role of CADM1 in ATL cells, we performed data base homology searches of all NCBI sequences looking for cytoplasmic proteins with type II PDZ domains similar to the PDZ domains of MAGUKs and found T-lymphoma invasion and metastasis 1 (Tiam1), which is a Rac-specific GEF. Amino acid sequence alignment revealed that among the members of MAGUKs, MPP2, Pals2 (MPP6), and CASK showed the closest similarity to the type II PDZ domain of Tiam1 (Fig. 1B). We analyzed, therefore, the expression of Tiam1 as well as CADM1 in both HTLV-I-transformed cell lines and ATL cell lines. As reported in an earlier study (8), CADM1 was specifically expressed in HTLV-I-transformed cell lines and ATL cell lines (Fig. 1C and supplemental Fig. S1, *middle*). In contrast, Tiam1 was detected not only in those cells but also in cell lines derived from HTLV-I-negative acute lymphoblastic T-cell leukemia and cutaneous T-cell lym-
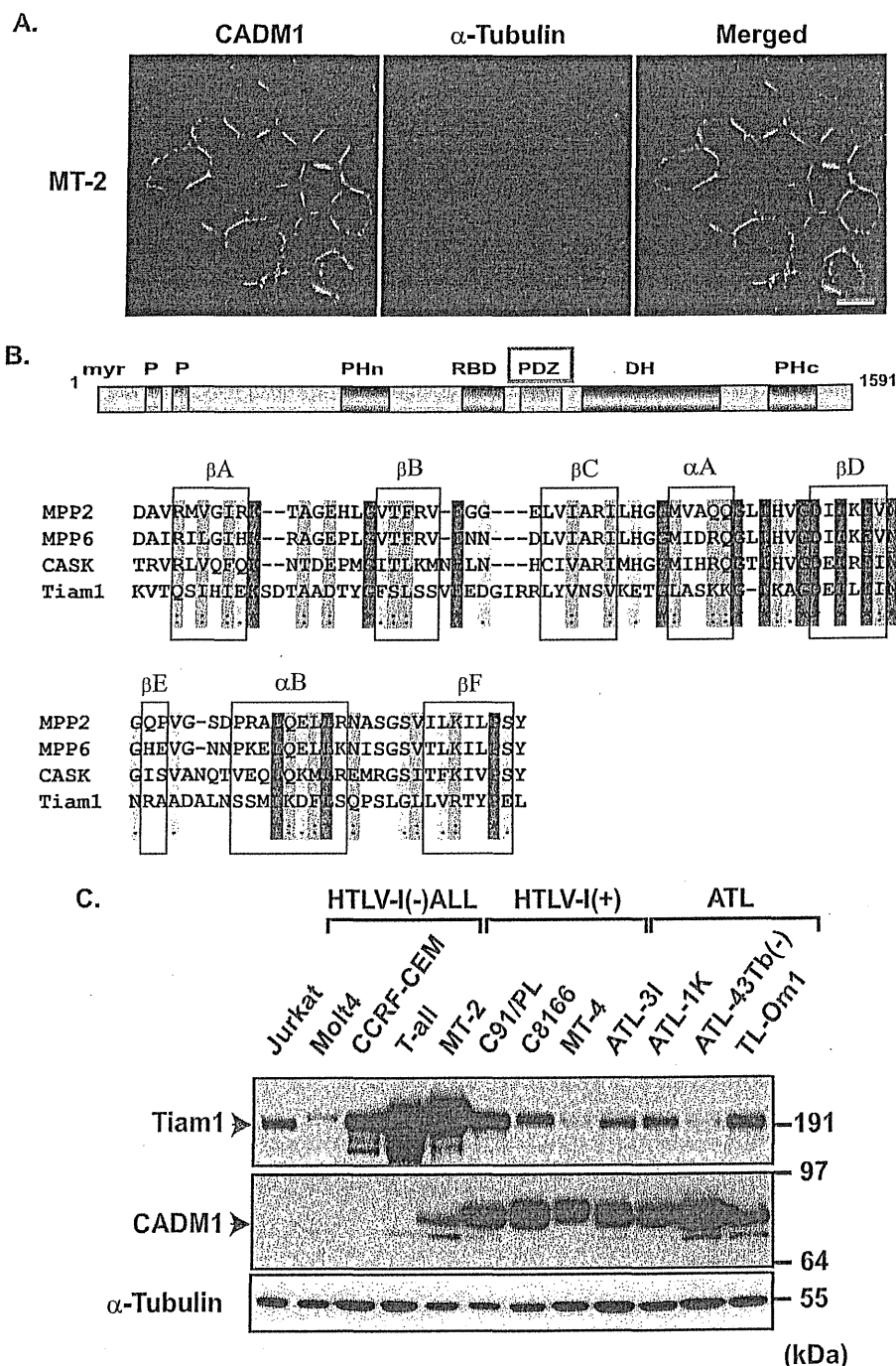
Interaction of CADM1 with Tiam1 in ATL Cells

FIGURE 1. **Expression of CADM1 and Tiam1 in HTLV-I-transformed cell lines and ATL cell lines.** A, expression of CADM1 in the HTLV-I-transformed cell line. MT-2 cells were immunostained for CADM1 (*green*) and α-tubulin (*red*) with a rabbit anti-CADM1 pAb (CC2) and a mouse anti-α-tubulin mAb and examined by confocal microscopy. *Scale bar*, 10 μm. Note that CADM1 is concentrated at the cell-cell attachment sites of the MT-2 cells. B, schematic representation of the domain structure of Tiam1 and sequence alignment of type II PDZ domains of selected MAGUKs and Tiam1. Tiam1 contains myristoylation signal (*myr*), Pest region (*P*), N-terminal pleckstrin homology domain (*PHn*), Ras-binding domain (*RBD*), type II PDZ (PSD-95/Dlg/ZO-1) domain (*PDZ*), Dbl homology domain (the catalytic domain) (*DH*), and C-terminal pleckstrin homology domain (*PHc*). Sequences were aligned using ClustalW. Conserved residues have been highlighted in *red*, and semiconserved residues are shown in *green* (very similar) and *yellow* (similar). The secondary structure elements, β-sheet and α-helix, are indicated as β and α. The GenBank™ data base accession numbers for the nucleotide sequences that encode human MPP2, MPP6, CASK, and Tiam1 are BC030287, NM016447, AF032119, and NM003253, respectively. C, immunoblot analysis for the expression of CADM1 and Tiam1 in acute lymphatic leukemia (*ALL*) cell lines, HTLV-I-transformed cell lines, and ATL cell lines. Five μg of cell lysates were fractionated in a 4–12% gradient NuPAGE Norvex BisTris gel, followed by immunoblot analysis as described under "Experimental Procedures." The antibodies used were a rabbit anti-Tiam1 pAb (C16) and a rabbit anti-CADM1 pAb (CC2). A mouse anti-α-tubulin mAb was used to show a loading control.

phoma (Fig. 1C and supplemental Fig. S1, *top*), indicating that expression of Tiam1 is not correlated with either HTLV-I infection or ATL. The molecular weight of CADM1 varied due to the difference in N-linked and O-linked glycosylation (data not shown).

Cytoplasmic Domain of CADM1 Interacts with Tiam1 in HTLV-I-transformed Cell Lines and ATL Cell Lines—We initially tested the physiological association of CADM1 with Tiam1 in a co-immunoprecipitation assay using an HTLV-I-transformed MT-2 cell line. When endogenous CADM1 was immunoprecipitated with a rabbit anti-CADM1 pAb (EC) from the MT-2 cell lysate, co-immunoprecipitation of endogenous Tiam1 was detected (Fig. 2A). Conversely, CADM1 was specifically detected in Tiam1 immunoprecipitate (Fig. 2A). The molecular weight of CADM1 co-precipitated with Tiam1 was slightly higher than the CADM1 signal detected in the MT-2 whole cell lysate (Fig. 2A), which may suggest that Tiam1 selectively interacts with heavily glycosylated CADM1 species. Reciprocal co-precipitation of CADM1 and Tiam1 was also observed in another HTLV-I-transformed cell line, C91/PL, as well as in an ATL cell line, ATL-3I (data not shown), proving that CADM1 was indeed associated with Tiam1 in those cells. N-terminal truncation of Tiam1 (C1199) (Fig. 2C, *left*) has been known to enhance its *in vitro* GEF activity and also has been suggested to increase the stability of Tiam1 due to the loss of PEST domains (Fig. 2C, *left*) that are believed to function as targeting signals to the degradation machinery (34). We examined, therefore, whether this active form of Tiam1, C1199, could associate with CADM1. A plasmid encoding either the full-length Tiam1 tagged with V5 (Tiam1-V5) or C1199 tagged with V5 (C1199-V5) was transfected into HEK293 cells, and both Tiam1-V5 and C1199-V5 were immunoprecipitated with a mouse anti-V5 mAb. Endogenous CADM1 was co-immunoprecipi-
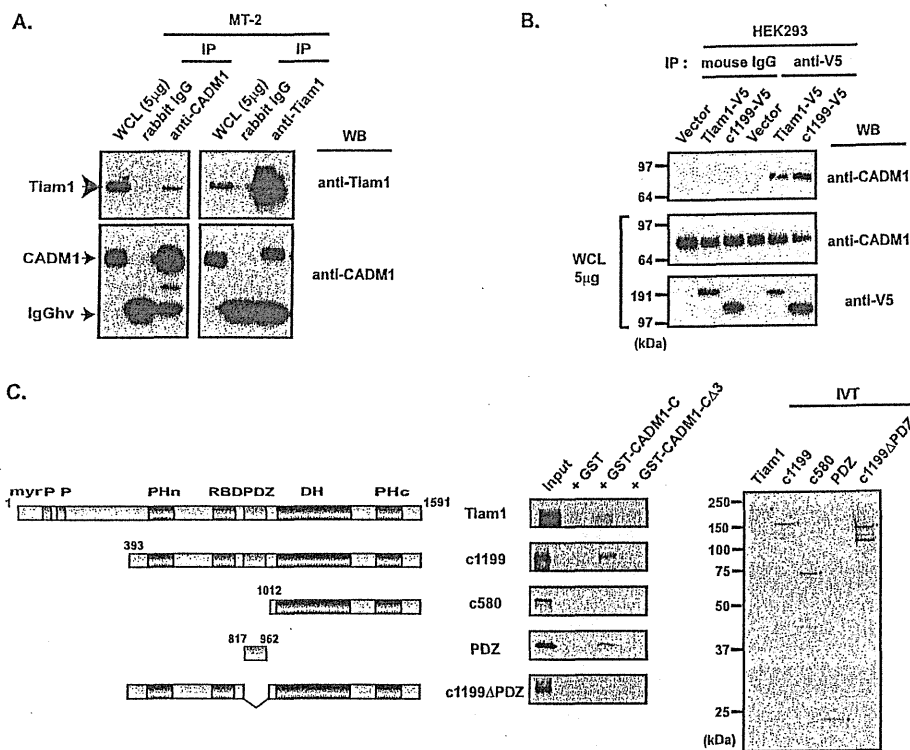
A.

B.

C.

FIGURE 2. **Direct interaction of CADM1 with Tiam1.** *A*, reciprocal co-immunoprecipitation of CADM1 with Tiam1 in the HTLV-I-transformed cell line, MT-2. Five hundred μg of cell lysates were immunoprecipitated (*IP*) with a rabbit anti-CADM1 pAb (*EC*), a rabbit anti-Tiam1 pAb (*C16*), or normal rabbit IgG. The precipitates were subjected to immunoblot analysis with the rabbit anti-Tiam1 pAb (*top*) and a rabbit anti-CADM1 pAb (*CC2*) (*bottom*). *Red, blue,* and *black arrows,* Tiam1, CADM1, and the rabbit IgG heavy chain, respectively. *B,* interaction of CADM1 with the active form of Tiam1 (C1199). Five hundred μg of cell lysates from HEK293 cells transiently transfected with pcDNA3.1, pcDNA/Tiam1-V5, or pcDNA/C1199-V5 were immunoprecipitated with a mouse anti-V5 mAb or normal mouse IgG and subjected to immunoblot analysis (*WB*) with CC2 (*top*). Five μg of whole cell lysates (*WCL*) were also analyzed for expression of CADM1 (*middle*), Tiam1-V5, and C1199-V5 (*bottom*) by immunoblot analysis with CC2 and anti-V5 mAb, respectively. *C,* the PDZ domain of Tiam1 is required for binding to the PDZ-BM of CADM1. The domain structure and truncated constructs of Tiam1 are shown on the *left*. GST, GST fused with the cytoplasmic domain of TSLC1, amino acids 392–442 (GST-CADM1-C), and GST fused with the cytoplasmic domain lacking C-terminal 3 amino acid residues, amino acids 392–439 (GST-CADM1-CΔ3), were expressed in *Escherichia coli.* [^{35}S]Methionine-labeled full-length and truncated Tiam1 were synthesized in reticulocytes. The size of the *in vitro* translated (*IVT*) proteins is shown in the *right panel* with *dots* indicating each full-length *in vitro* translated product. For *in vitro* binding, labeled proteins were incubated with GST or GST fusion protein immobilized on glutathione-Sepharose beads and subjected to SDS-PAGE. Binding of ^{35}S-labeled proteins was detected by autoradiography (*middle column*). The entire images of the GST pull-down assay are shown in supplemental Fig. S2.

tated not only with Tiam1-V5 but also with C1199-V5 (Fig. 2*B*) in HEK293 cells, indicating that C1199 interacted with CADM1. We next analyzed whether Tiam1 would directly bind to the cytoplasmic domain of CADM1 by a GST pull-down assay using various truncation mutants of Tiam1 that were translated as V5-tagged proteins in rabbit reticulocyte lysates containing [^{35}S]methionine. The bacterially expressed GST protein fused with the cytoplasmic domain of CADM1 (GST-CADM1-C) was precipitated with full-length Tiam1 and C1199 but not with C580, indicating that the cytoplasmic domain of CADM1 directly interacted with Tiam1, and amino acid residues between 393 and 1012 of Tiam1 were essential for this direct interaction between CADM1 and Tiam1 (Fig. 2*C* and supplemental Fig. S2). We further identified the PDZ domain of Tiam1 as the region responsible for the CADM1 binding. Although the PDZ tightly bound to GST-CADM1-C, deleting the PDZ domain from C1199 (C1199ΔPDZ) was enough to abolish the interaction

between C1199-C5 and GST-CADM1-C (Fig. 2*C* and supplemental Fig. S2). In contrast, GST protein fused with the cytoplasmic domain of CADM1 lacking the 3 C-terminal amino acids (GST-CADM1-CΔ3) did not associate with either C1199, C580, or PDZ, thus demonstrating that the PDZ-BM of CADM1 was sufficient for the direct interaction between Tiam1 and CADM1.

Cytoplasmic Domain of CADM1 Induces Formation of Lamellipodia through Rac Activation in Jurkat Tet-off Cells Expressing CADM1—In an attempt to assess the role of CADM1 in the infiltration of ATL cells into tissue, we established doxycycline (Dox)-inducible acute lymphoblastic T-cell leukemia Jurkat cell clones expressing CADM1 (Jurkat/CADM1). In the isolated Jurkat/CADM1 cell clone, expression of CADM1 was tightly regulated with Dox (Fig. 3*A*). Expression of CADM1 induced extensive formation of cell aggregates in Jurkat cells (Fig. 3*A, bottom right*) that were reminiscent of cell aggregates seen in HTLV-I-transformed cell lines, such as MT-2 cells (Fig. 1*A*), and ATL cell lines indicating that homophilic *trans*-interaction of CADM1 mediated formation of cell aggregates in Jurkat cells. It appears that homophilic *trans*-interaction of CADM1, therefore, contributes to formation of aggregates in many of the HTLV-I-transformed cell lines and ATL cell lines. In Jurkat/CADM1 cells, co-immunoprecipitation of endogenous Tiam1 was also confirmed in the precipitate with anti-CADM1 pAb (EC) (Fig. 3*B*). We next examined localization of CADM1 and Tiam1 in Jurkat/CADM1 cells co-cultured on a monolayer of mouse NIH3T3 fibroblasts for 7 h. In the absence of Dox, Jurkat cells expressing CADM1 tightly adhered to and spread over the monolayer of fibroblasts, forming lamellipodia where CADM1 and Tiam1 were co-localized (Fig. 3*C, middle* and *bottom*). In contrast, Jurkat/CADM1 cells in which CADM1 expression was repressed with Dox neither infiltrated into the monolayer of fibroblasts nor formed membrane ruffles at the cell edge, and Tiam1 was distributed in the cytoplasm of those cells (Fig. 3*C, top panels*). These findings together demonstrated that CADM1 could induce formation of lamellipodia and recruit Tiam1 at the periphery of the lamellipodia. Such effects by CADM1 required its cytoplasmic domain because the deletion mutant lacking the cytoplasmic domain of CADM1 could not

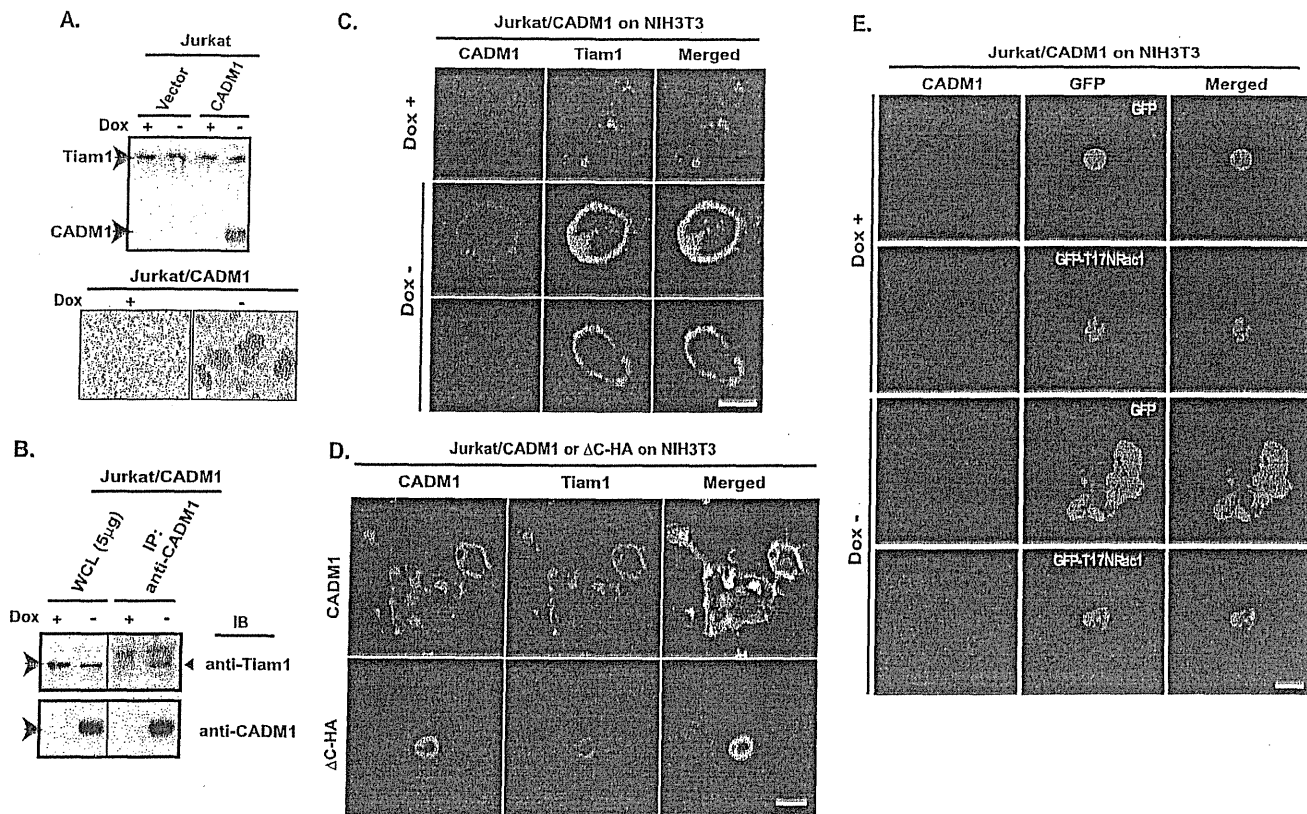# Interaction of CADM1 with Tiam1 in ATL Cells

FIGURE 3. The cytoplasmic domain of CADM1 is necessary for formation of lamellipodia in Tet-off Jurkat cells cultured on NIH3T3 fibroblasts. *A*, inducible expression of CADM1 in Tet-off Jurkat cells. The established Tet-off Jurkat cell clones, Jurkat/vector and Jurkat/CADM1, were cultured in the presence (+) and absence (−) of 100 μg/ml Dox for 5 days. Five μg of cell lysates were subjected to immunoblot analysis with an anti-CADM1 pAb (CC2) and anti-Tiam1 pAb (C16) as shown in the *top panel*. The *red* and *blue arrows* indicate Tiam1 and CADM1, respectively. Representative phase-contrast images of Jurkat/CADM1 cells cultured in media with or without 100 μg/ml Dox for 5 days are shown in the *bottom panels*. Original magnification was ×100. Note that CADM1-expressing Jurkat/CADM1 cells show extensive aggregates. *B*, co-immunoprecipitation of CADM1 with Tiam1 in the Tet-off Jurkat/CADM1 cells. The Jurkat/CADM1 cells were cultured in the presence (+) and absence (−) of 100 μg/ml Dox for 5 days. To confirm the expression of Tiam1 and CADM1, 5 μg of whole cell lysates (*WCL*) were subjected to immunoblot analysis (*left halves of panels*). Five hundred μg of cell lysates were immunoprecipitated (*IP*) with an anti-CADM1 pAb (EC) and subjected to immunoblot analysis for Tiam1 with C16 (*right half of top panel*) and for CADM1 with CC2 (*right half of the bottom panel*). Co-precipitated Tiam1 is indicated with a *black arrowhead*. The *red* and *blue arrows* indicate Tiam1 and CADM1, respectively. *C*, CADM1 is necessary for formation of lamellipodia in Jurkat cells cultured on NIH3T3 fibroblasts. Jurkat/CADM1 cells were co-cultured on a monolayer of NIH3T3 cells for 17 h. The cells were stained for CADM1 (*blue*) and Tiam1 (*green*) with a chicken anti-CADM1 mAb (3E1) and an anti-Tiam1 pAb (C16), respectively. *Magnified images* show that CADM1 and Tiam1 are detected at membrane ruffling areas (*middle* and *bottom panels*). *Scale bar*, 10 μm. *D*, cytoplasmic domain of CADM1 induces formation of lamellipodia. Jurkat/CADM1 and Jurkat/ΔC-HA were seeded on NIH3T3 monolayers and incubated for 17 h. Cells were triple-stained for CADM1 (*green*), Tiam1 (*red*), and actin (*blue*). Actin filaments are shown in the *merged panels*. Note that stress fibers of NIH3T3 cells are seen in the *top merged panel*, indicating that Jurkat/CADM1 cells infiltrated into the NIH3T3 monolayer. *Scale bar*, 10 μm. *E*, a dominant negative mutant of Rac1, T17NRac1, blocked CADM1-induced formation of lamellipodia. Jurkat/CADM1 cells cultured in the presence (+) or absence (−) of 100 μg/ml Dox for 5 days were transiently transfected with pEGFP or pEGFP-T17NRac1. The next day, the transfected cells were seeded on NIH3T3 monolayers and incubated for 17 h. Cells were stained for CADM1 (*blue*). *Scale bar*, 10 μm.

induce formation of lamellipodia in Jurkat cells co-cultured on the monolayer of fibroblasts (Fig. 3*D*). In addition, Tiam1 did not accumulate at the cell periphery of these cells, suggesting that the interaction of the cytoplasmic domain of CADM1 and Tiam1 was necessary for the formation of lamellipodia (Fig. 3*D*). Because Tiam1 is known to be a Rac-specific GEF, we also tested whether activation of Rac was needed for CADM1-induced formation of lamellipodia by introducing a dominant negative mutant of Rac tagged with green fluorescent protein (T17NRac1-GFP) in Jurkat/CADM1 cells. T17NRac1-GFP completely blocked CADM1-induced formation of lamellipodia (Fig. 3*E*), thereby underscoring the importance of Rac activation presumably through Tiam1 in CADM1-induced formation of lamellipodia.

CADM1 and Tiam1 Co-localizes at the Leading Edge of Migrating ATL-3I Cells—Infiltration of ATL cells into various kinds of tissue like skin involves several key steps: 1) adhesion to

endothelial cells; 2) transmigration of vessel walls; 3) crawling into dermis where fibroblasts are abundant; and 4) epidermal localization. We looked, therefore, into the localization of CADM1 and Tiam1 in ATL cell lines co-cultured on either HMVEC or NHDF. After a 17-h co-culture of the ATL cell line, ATL-3I, on top of the monolayer of HMVEC, the cells firmly adhered to HMVEC and formed lamellipodia where CADM1 and Tiam1 were intensely co-accumulated (Fig. 4*A* and supplemental Fig. S3). ATL-3I cells adhered to a NHDF monolayer in shorter 6-h co-culture (Fig. 4, *C* and *D*) and exhibited lamellipodia in most of the cells adhered to NHDF where co-localization of CADM1 and Tiam1 was seen (Fig. 4*D*). As observed in Jurkat/CADM1 cells overlaid on NIH3T3 cells, a dominant negative T17NRac1 mutant also inhibited the formation of lamellipodia in ATL-3I cells on HMVEC, suggesting that Rac activity was required for ATL-3I cells to tightly attach to the monolayer of HMVEC and subsequently form lamellipodia
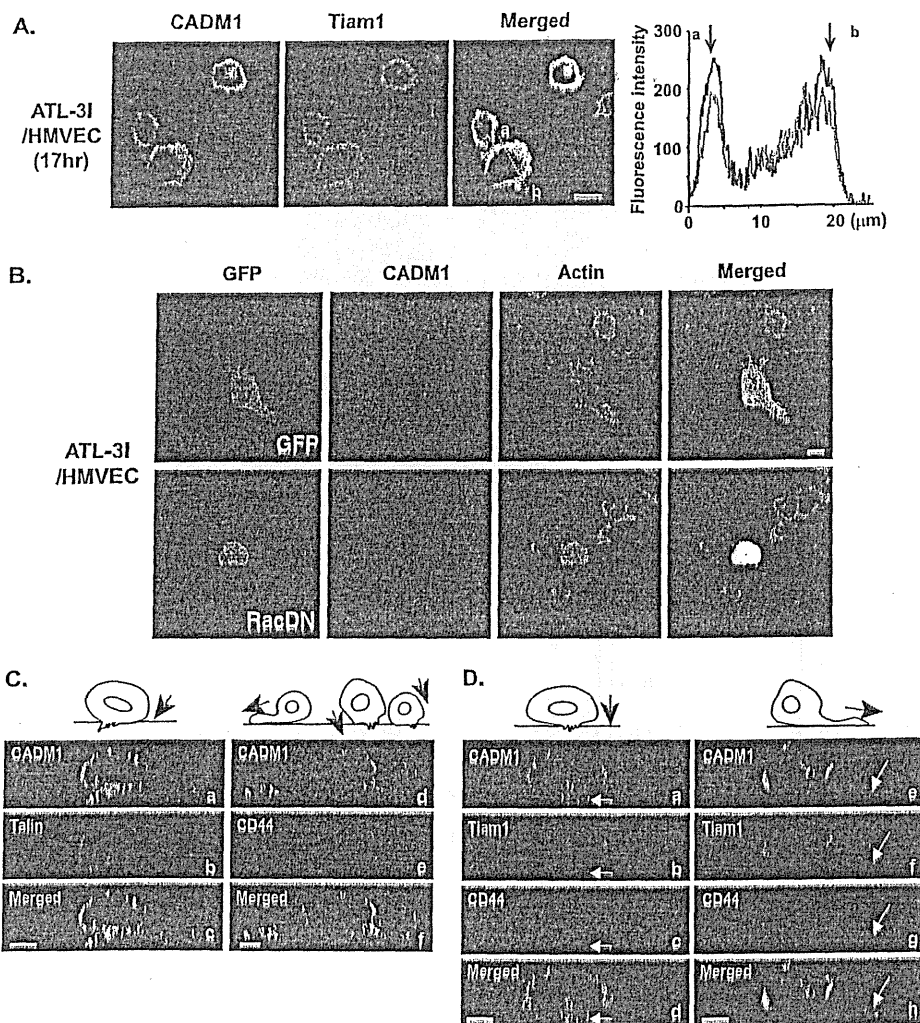
A.

B.

C. **D.**

FIGURE 4. **CADM1 and Tiam1 are co-localized at the leading edge of ATL-3I cells.** *A,* co-localization of CADM1 with Tiam1 at the peripheral margin of ATL-3I cells. Cells were seeded on a monolayer of HMVEC and cultured for 17 h. Cells were double-stained for CADM1 *(green)* and Tiam1 *(red)* with a chicken anti-CADM1 mAb (3E1) and a rabbit anti-Tiam1 pAb (C16), respectively, and then examined by confocal microscopy. *Scale bar,* 10 µm. A line scan graph of CADM1 *(green)* and Tiam1 *(red)* fluorescence intensities is shown. Fluorescence intensities were measured along a *white dotted line* from *a* to *b* in the *merged* panel. The *arrows* in the *graph* indicate the position of the cell edges. The patterns of CADM1 and Tiam1 intensities are similar and high at the edges of the cell. *B,* a dominant negative mutant of Rac1, T17NRac1, blocked CADM1-induced formation of lamellipodia. ATL-3I cells transfected with pEGFP or pEGFP-T17NRac1 were co-cultured on an HMVEC monolayer for 17 h and stained for CADM1 *(blue)* and actin *(red)*. *Scale bar,* 10 µm. *C,* CADM1 co-localized with the leading edge marker Talin but not with the trailing edge marker CD44 at the invasive front of ATL3I cells. *a–f, xz* sections of ATL3I cells adhered to NHDF. CADM1 was co-localized with Talin *(a–c)* but not with CD44 *(d–f)* at the invasive front of ATL3I cells. ATL-3I cells co-cultured on a NHDF monolayer for 6 h were double-stained for CADM1 *(green)* and Talin *(red* in *b* and *c)* or CD44 *(red* in *e* and *f)* with 3E1 and a mouse anti-Talin mAb or mouse anti-CD44 mAb (C26), respectively. Note that intense staining of CADM1, not CD44, is seen at the adhesion sites of ATL-3I cells to NHDF. Illustrations of the cells are depicted *above* the *top panels (a* and *d)* with *red arrows* that indicate the direction of cell migration. *Scale bar,* 10 µm. *D,* CADM1 and Tiam1 co-localized at the invasive front of ATL3I cells. *a–h, xz* sections of ATL cells attached to the NHDF monolayer. Cells were triple-stained for CADM1 *(green)*, Tiam1 *(red)*, and CD44 *(blue)* with 3E1, C16, and C26, respectively. The *white arrows* show co-localization of CADM1 and Tiam1 at the ventral surface of ATL-3I cells invading the NHDF monolayer *(a–d)* and at the leading edge of ATL-3I cells adhering to the monolayer *(e–h)*. Illustrations of the cells are depicted *above* the *top panels (a* and *e)* with *red arrows* that indicate the direction of cell migration. *Scale bars,* 5 µm.

(Fig. 4*B*). We realize that the first requirement for a cell to initiate migration is the acquisition of polarized morphology, and establishment of cell polarity occurs during the migration of lymphocytes (35). In ATL-3I cells adhered to NHDF, therefore, we compared the distribution of CADM1 with that of Talin and CD44, which are well established markers for the leading and trailing edges of chemokine-induced migratory T

lymphocytes, respectively. *xz* cross-section analysis of these cells revealed that intense staining of CADM1 and Talin was detected at the contact zones of ATL-3I cells to NHDF (Fig. 4*C, a–c*). In contrast, CD44 was not observed in those contact regions (Fig. 4*C, d–f*), indicative of CADM1 localization at the leading edge of the migrating cells. Triple immunofluorescence staining for CADM1, Tiam1, and CD44 in the *xz* cross-section of such cells revealed that CADM1 was completely co-localized with Tiam1 at the cell periphery (Fig. 4*D, a–d* and *e–h*). At the adhering sites of ATL-3I cells to NHDF, however, CADM1 was co-localized with Tiam1, but not with CD44 (Fig. 4*D, a–d* and *e–h*), demonstrating that CADM1 and Tiam1 were distributed at the leading edge of polarized migrating cells. This was further confirmed by quantitative analysis of the *xz* cross-sections of the adhering area of ATL-3I cells to NHDF monolayers. Thirty-seven of 40 (93%) ATL-3I cells showed CADM1/Tiam1-double-positive and CD44-negative adhering sites.

Both CADM1 and Tiam1 Are Necessary for Lamellipodium Formation of HTLV-I-transformed and ATL Cell Lines—To further substantiate the importance of CADM1 and Tiam1 in CADM1-induced formation of lamellipodia, we introduced either CADM1 or Tiam1 siRNA into HTLV-I-transformed cell lines, C91/PL and MT-4, and an ATL cell line, ATL-3I. Immunoblot analysis of CADM1 and Tiam1 protein revealed that decreases in CADM1 and Tiam1 were most prominent in C91/PL cells (Fig. 5*A*) due to them having the highest transfection efficiency among the three cell lines (data not shown). Forty-eight h after the introduction of siRNA, the cells in which CADM1 expression had been knocked down lost their aggregate morphology and started growing as single cells (Fig. 5*B, upper middle* and *right panels*), whereas siRNA-mediated knockdown of Tiam1 interfered with aggregate formation to a much lesser extent (Fig. 5*B, bottom panels*). It should be noted that disruption of cell aggregation in ATL3I cells by CADM1 knockdown was not as striking as in MT-4 cells (data not

Interaction of CADM1 with Tiam1 in ATL Cells
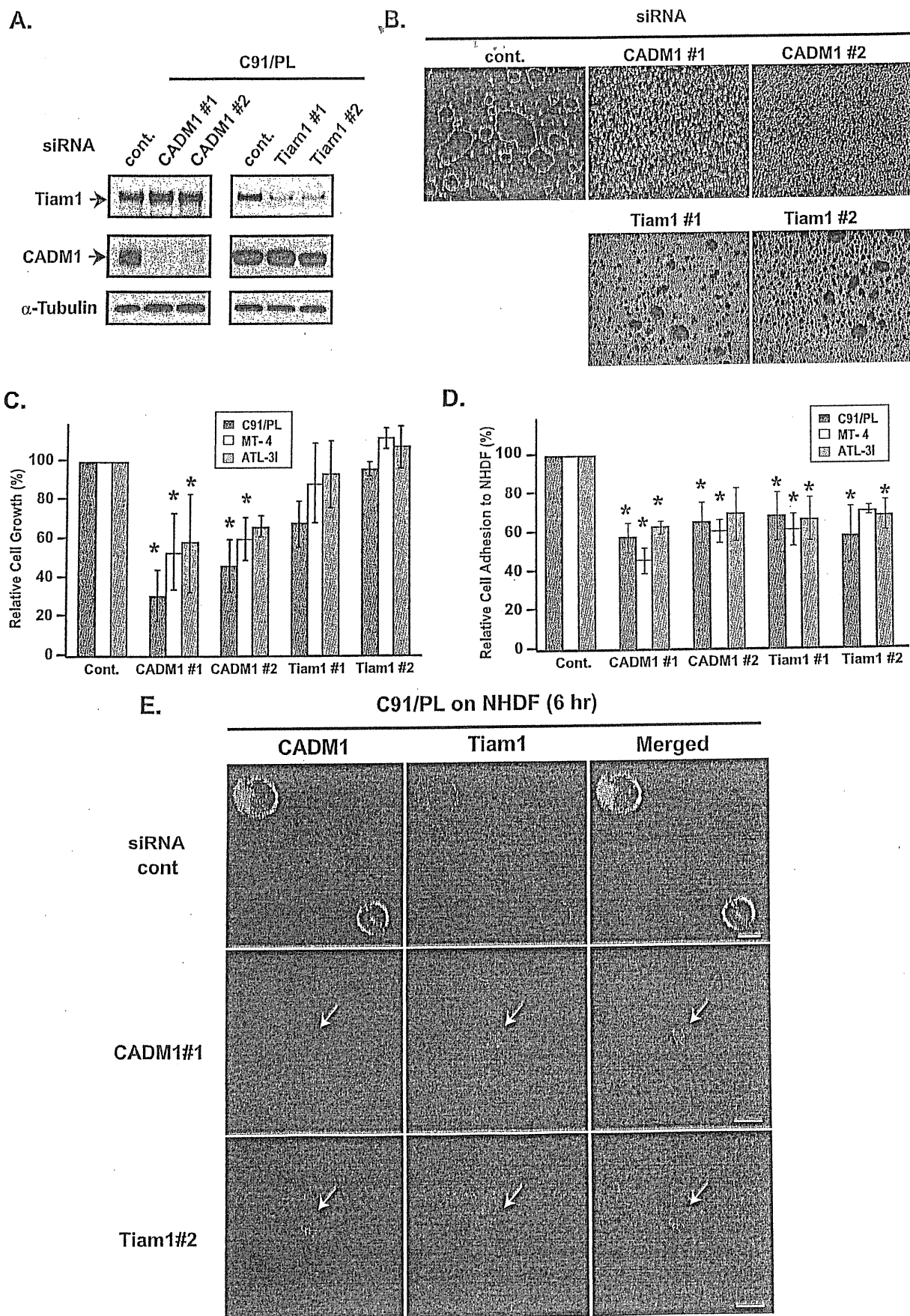
A.

siRNA

Tiam1 →

CADM1 →

α-Tubulin

B.

siRNA

C.

D.

E.

C91/PL on NHDF (6 hr)

shown), suggesting that other adhesion molecules are also involved in cell aggregation of HTLV-I-transformed cell lines and ATL cell lines. In assessing whether the reduction in aggregate formation influenced cell growth, we counted the number of living cells 7 days after siRNA introduction and found that knockdown of CADM1 dramatically reduced cell growth of C91/PL cells to ~30% (Fig. 5C). Although not as strongly as in C91/PL cells, cell growth of MT-4 and ATL-3I cells was also decreased from 50 to 66% upon silencing of CADM1 (Fig. 5C). In contrast, knockdown of Tiam1 did not affect cell growth at levels comparable with those induced by knockdown of CADM1 (Fig. 5C). Together, these indicate that CADM1 enhanced the cell growth of both HTLV-I-transformed cell lines and an ATL cell line by mediating formation of cell aggregates through homophilic *trans*-interaction of CADM1, but it is unlikely that Tiam1 was involved in the effect. We further analyzed whether CADM1 or Tiam1 was necessary for adhesion to NHDF and subsequent formation of lamellipodia on NHDF. An adhesion assay of a 2-h co-culture of these ATL cell lines on a NHDF monolayer showed that knockdown of either CADM1 or Tiam1 reduced the level of cell adhesion by a similar amount (50–70%) (Fig. 5D). This result was consistent with the immunofluorescent microscopic observation, which showed that siRNA-mediated knockdown of CADM1 and Tiam1 in C91/PL cells on NHDF repressed formation of lamellipodia and abrogated cell periphery localization of Tiam1 and CADM, respectively (Fig. 5E). These data together indicate that either Tiam1 or CADM1 are necessary for formation of lamellipodia in HTLV-I-transformed cell lines and ATL cell lines.

Co-localization of CADM1 and Tiam1 in Lymph Node Lesions of ATL Patients—Finally, we examined the expression of CADM1 and Tiam1 in lymph node lesions from nine ATL patients with lymph node involvement by immunohistochemistry. As representatively shown in Fig. 6A, infiltrating tumor cells demonstrated immunoreactivity for CADM1 in eight of the nine patients tested (four strongly positive, four positive, and one negative). In comparison, Tiam1 was detected in three patients who also were positive for CADM1, indicating that one-third of the specimens from those nine ATL patients were double-positive. Immunohistostaining revealed that CADM1 was detected at the plasma membrane of the tumor cells (Fig. 6A, left column), and aggregate accumulation of CADM1 was seen in some cases as an intense punctate structure (Fig. 6A, bottom left panel). Tiam1 was observed not only at the membrane but also in the cytoplasm of the infiltrating ATL cells (Fig.
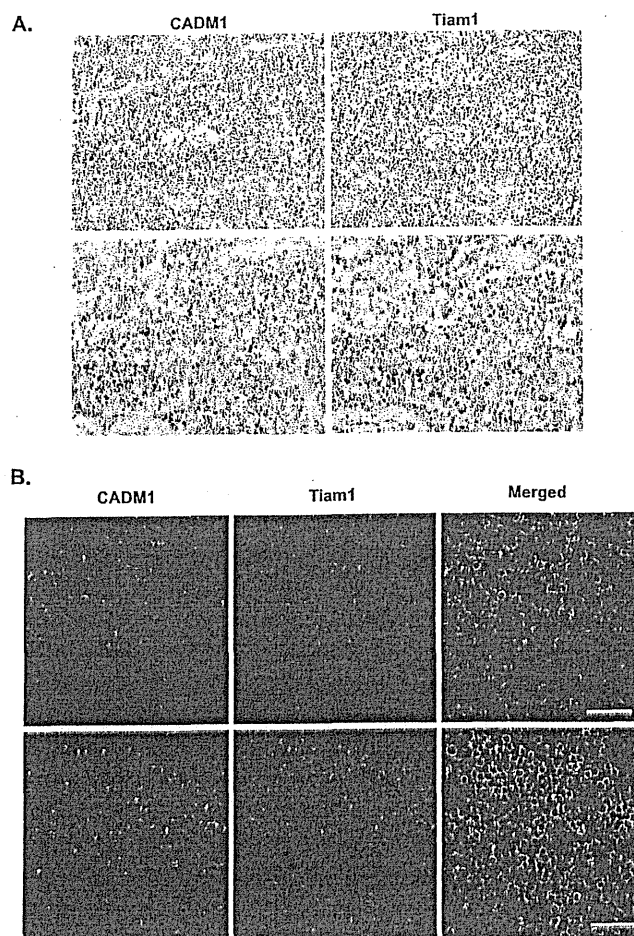

FIGURE 6. Co-localization of CADM1 and Tiam1 in lymph node lesions of ATL patients. A, immunohistochemical staining for CADM1 and Tiam1. Tissues were incubated with a rabbit anti-CADM1 pAb (number 6) (*left panels*) or a rabbit anti-Tiam1 pAb (C16) (*right panels*) and stained with aminoethylcarbazole. The nuclei were counterstained with hematoxylin. Representative images of the CADM1^{+}/Tiam1^{+} specimens are shown. Original magnification was ×200 (*top panels*) and ×400 (*bottom panels*). B, co-localization of CADM1 and Tiam1 at the cell membrane of infiltrating ATL cells. Immunofluorescence double-staining of sections for CADM1 (*green*) and Tiam1 (*red*) was performed with a chicken anti-CADM1 mAb (3E1) and a rabbit anti-Tiam1 pAb (C16). *Scale bars*, 50 μm.

6A, *right column*). In an effort to determine more precisely whether CADM1 and Tiam1 co-localize, we performed immunofluorescence double-staining. Although none of the Tiam1-positive specimens showed a unique pattern of punctate structure-like distribution of CADM1 as seen in Fig. 6A, CADM1

FIGURE 5. Both CADM1 and Tiam1 are required for formation of lamellipodia in HTLV-I-transformed cell lines and ATL cell lines. A, siRNA-mediated CADM1 and Tiam1 knockdown. Control siRNA (*cont*), CADM1-specific siRNA (*CADM1 1* and *CADM1 2*), or Tiam1-specific siRNA (*Tiam1 1* and *Tiam1 2*) was introduced into C91/PL cells with electroporation. Forty-eight h after electroporation, lysates were prepared, and 5 μg of the lysates were analyzed by immunoblot with anti-CADM1 pAb (CC2) and anti-Tiam1 pAb (C16). Signals of α-tubulin are shown as loading controls in the *bottom panel*. The *red* and *blue arrows* indicate Tiam1 and CADM1, respectively. B, CADM1 knockdown disrupted cell aggregates of MT-4 cells. Phase-contrast images were taken 48 h after introduction of siRNA CADM1 by electroporation. Note that although similar results were obtained in C91/PL cells and ATL-3I cells, disruption of cell aggregates by CADM1 knockdown was most prominent in MT-4 cells. Original magnification was ×100. C, CADM1 knockdown reduced cell growth of C91/PL, MT-4, and ATL-3I cells. Seven days after electroporation, living cells were counted by trypan blue dye exclusion. Each *bar* represents the mean ± S.D. (*error bars*) of triplicate assays. The *asterisks* indicate statistical significance with $p < 0.05$ as determined by Student's t test. D, either CADM1 or Tiam1 knockdown impaired cell adhesion to NHDF monolayers. Forty-eight h after electroporation, calcein AM-labeled cells were co-cultured on NHDF monolayers for 2 h. Each *bar* represents the mean ± S.D. of three independent experiments. The *asterisks* indicate statistical significance with $p < 0.05$ as determined by Student's t test. E, either CADM1 or Tiam1 knockdown abrogated lamellipodium formation of C91/PL cells cultured on a NHDF monolayer. C91/PL cells treated with specified siRNA were co-cultured on NHDF monolayers for 6 h. Cells were double-stained for CADM1 (*green*) and Tiam1 (*red*) with a chicken anti-CADM1 mAb (3E1) and a rabbit anti-Tiam1 pAb (C16), respectively. *Scale bars*, 10 μm. Note that either CADM1 knockdown or Tiam1 knockdown not only inhibits formation of lamellipodia but also affects the membrane localization of Tiam1 or CADM1.

and Tiam1 were well co-localized at the cell membrane of ATL cells (Fig. 6B). When considered together, these data support our finding *in vitro* that both CADM1 and Tiam1 are cooperatively involved in the infiltration of ATL cells.

DISCUSSION

In this study, we identified Rac-specific GEF, Tiam1, as a binding partner of CADM1 in both HTLV-I-transformed and ATL-derived cell lines and demonstrated that the interaction induced formation of lamellipodia, structures seen at the leading edge of motile cells, indicating that CADM1-Tiam1 interaction was involved in the infiltrative propensity of ATL cells. Although the cohort of ATL patients we investigated was not large enough to provide conclusive clinical evidence, CADM1 and Tiam1 were well co-localized at the cell membrane in the Tiam1$^+$/CADM1$^+$ specimens from ATL patients with lymph node involvement. In normal T lymphocytes in which CADM1 is barely detectable (8), Tiam1 regulates chemokine-induced T-cell polarization and chemotaxis by associating with the Par3-Par6-atypical protein kinase C polarity complex (36). In ATL cells, the overexpressed CADM1 interacts with Tiam1 through the type II PDZ-BM of CADM1 and recruits Tiam1 to the intracellular submembranous domain. Rac-specific guanine nucleotide exchange factor activity of Tiam1 is known to depend on the membrane localization of Tiam1, which is mediated by binding to phosphoinositides through the N-terminal pleckstrin homology domain (*PHn*) of Tiam1 (Fig. 1B) (37). Others have reported, however, that the N-terminal pleckstrin homology domain of Tiam1 possesses a relatively weak affinity and less specificity for phosphoinositide compared with the pleckstrin homology domains of PLCδ and Akt (38), indicating that binding of the N-terminal pleckstrin homology domain with phosphoinositide seems to play an accessory but not a defining role in targeting Tiam1 to cell membranes. It is, therefore, likely that the interaction of Tiam1 with transmembrane proteins facilitates its membrane localization. Furthermore, these transmembrane proteins with which Tiam1 interacts may determine the downstream signals subsequently triggered by such interaction. Accordingly, the association of CADM1 with the PDZ domain of Tiam1 could reinforce tethering of Tiam1 to the membrane and induce the signal specific to CADM1. We have previously shown that CADM1 binds to actin through its protein 4.1-BM (14). CADM1, therefore, seems to recruit actin and a regulator of actin, the Rac-specific guanine nucleotide exchange factor, together to the juxtamembrane region, thereby becoming a powerful driving force for actin reorganization to induce cell motility (Fig. 7). As can be surmised, co-expression of CADM1 and Tiam1 in T lymphocytes appears to be an unwanted combination that leads to the deviated invasive tendencies of ATL cells.

Regardless of its tumor suppressor activities in various cancers (1, 33), our study revealed that CADM1 functions rather as an oncoprotein in ATL. Intriguingly, similar complexity of paradoxical functions has been well illustrated in Tiam1 (39). Besides promoting invasion of T-cell lymphoma cells (20, 40), Tiam1 expression has been demonstrated to correlate with the invasive and metastatic phenotypes of breast and colon cancers (39). It has also been shown that Tiam1$^{-/-}$ mice are resistant to
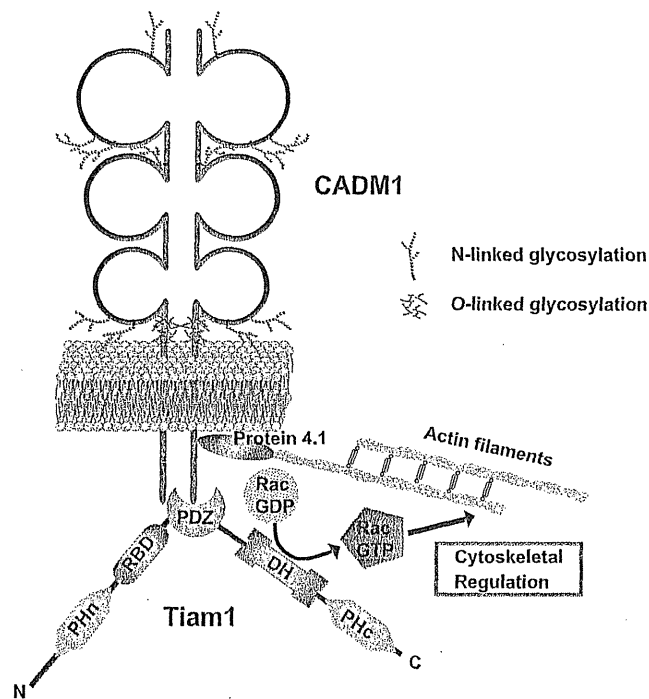

CADM1

$\ \ $ N-linked glycosylation

$\ \ $ O-linked glycosylation

FIGURE 7. **A possible role of CADM1 in ATL cells.** CADM1 comprises three Ig loops modified with *N*-linked and *O*-linked glycosylation, a single membrane-spanning α-helix, and a short cytoplasmic domain. The cytoplasmic domain has a protein 4.1-BM connected to the actin cytoskeleton through members of the protein 4.1 family and a type II PDZ-BM interacting with Tiam1. CADM1, therefore, seems to recruit actin and a regulator of actin, the Rac-specific *guanine nucleotide exchange factor, together* to the juxtamembrane region, leading to Rac activation for actin reorganization. Domains of Tiam1 are abbreviated as described in the legend to Fig. 1B.

the development of Ras-induced skin tumors, suggesting that Tiam1 contributes to tumorigenicity (41). As opposed to these abilities of Tiam1 to promote invasion and metastasis as well as tumor formation, Tiam1 expression has been demonstrated to be inversely correlated with the invasive potential of renal cell carcinoma cell lines (42). Such contradictory findings are proposed to be due to the effects of Tiam1, which solely depend on the cell type and the Rho GTPase activation status in the particular spatio-temporal context of given cells (39). It is plausible, therefore, that the dualistic effects of CADM1 may be also attributable to the cell type and activation state of Rho GTPs. In fact, we previously demonstrated using epithelial Madin-Darby canine kidney cells that the cytoplasmic domain of CADM1 induced prolonged activation of Rac and reduced activation of Rho, leading to suppression of hepatocyte growth factor-induced epithelial mesenchymal transitions, which is a crucial step for tumor cells to become invasive (30). Coincidentally, ectopic expression of Tiam1 or constitutively active Rac was reported to block hepatocyte growth factor-induced cell scattering of Madin-Darby canine kidney cells with high Rac and low Rho activities(43). It is tempting to speculate, therefore, that CADM1 spatio-temporally associates with Tiam1 even in some epithelial cells where they cooperatively work together as a tumor suppressor by maintaining epithelial integrity.

Although it is becoming increasingly clear that adhesion molecules are involved in transendothelial migration of leukocytes, this may not be the only possible process in which

CADM1 is involved in infiltration of ATL cells into various organs and tissues, such as skin. Skin involvement is one of the most frequent manifestations in ATL patients. The extracellular domain of CADM1 is known to interact homophilically with itself (6, 7), as well as heterophilically with CADM2 (Necl-3) (44), CADM3 (Necl-1) (6), Nectin-3 (6) and CRTAM (45–47). The molecular interactions that facilitate ATL migration to and retention in skin may involve various cells residing in the skin that express those ligands for CADM1. Such cells may include mast cells that are immune cell residents of the dermis constitutively expressing CADM1 (48). Our study revealed that ATL cells adhered to NHDF with even higher affinity than to HMVEC. NHDF are abundant in epidermis and quite possibly help ATL cells to crawl into the dermal interstitium. We have found that CADM1-positive cells tend to show a high affinity with fibroblasts, which are CADM1-negative, suggesting that fibroblasts express some of those heterophilic ligands described above or as yet unidentified ligands for CADM1. ATL cells often display an affinity for Langerhans cells, immature dermal dendritic cells, and cluster around them in the epidermis forming Pautrier's microabscesses (49). Because CADM1 is known to define a certain subset of dendritic cells (45), it is possible that Langerhans cells express CADM1, thereby attracting ATL cells to the epidermis. It is noteworthy that the dermis is abundant in sensory nerve fibers that constitute an elaborate network. Other than CRTAM, the CADM1 ligands listed above are copiously expressed in nerve cells (5, 44). It seems plausible, therefore, that ATL infiltration into skin is promoted through the interaction between ATL cells and nerve fibers. It remains elusive, however, whether the CADM1-Tiam1-Rac cascade is constitutively activated in ATL cells or the activation is triggered by adhesion of ATL cells to the cells expressing those CADM1 ligands mentioned above. Further studies to define the mechanism of CADM1 activation of Rac through Tiam1 are now ongoing. Because phosphorylation of Tiam1 on its serine/threonine and tyrosine residues was previously reported (34, 39), investigating spatio-temporal phosphorylation of Tiam1 in HTLV-I-transformed and ATL-derived cell lines would provide pivotal information toward understanding the CADM1-Tiam1-Rac signaling in ATL cells.

In the present study, we found that CADM1 knockdown affected cell growth, suggesting that CADM1 may play an auxiliary role in transformation of HTLV-I-infected T cells. During such a transformation stage, Tiam1 may not be the sole binding partner of CADM1 because Tiam1 knockdown did not have an effect on cell growth. Tax is reported to be directly associated with small Rho GTPase and therefore is believed to play a role in the infiltrating propensity of ATL cells (18, 50). It is known, however, that Tax expression is frequently lost in ATL cells (51). In contrast, a previous study from others (8) reported that CADM1 was expressed in all of the primary ATL cells tested. In such Tax-negative ATL cells, CADM1-Tiam1 interaction may become one of the driving forces for cytoskeletal reorganization, thereby contributing to the infiltrating phenotype of ATL cells. In support of this, it has been reported that, compared with ED, the CADM1-nagative ATL cell line, ED cells overexpressing CADM1 caused larger tumor formation and massive infiltration into various organs in NOG mice (52).

Elucidating the molecular mechanisms of the CADM1-Tiam1 pathway involved in tissue infiltration of ATL cells may offer alternative approaches to the treatment of ATL, such as specific interference with CADM1 using a mAb against the ectodomain of CADM1. The use of therapeutic mAb for the treatment of cancer has shown promising results over the past few years, as exemplified by the major success of a mAb against HER2 in treatments for metastatic breast cancer and lung cancer. Our study revealed that CADM1 affected both lamellipodium formation and cell growth, thus suggesting that interference with CADM1 may inhibit not only tissue infiltration of ATL cells but also the growth of ATL cells. Tiam1 may also become an attractive pharmacological target for developing small molecular inhibitors of the invasive nature of ATL cells by manipulating the CADM1-Tiam1-Rac signaling pathways.

REFERENCES

1. Kuramochi, M., Fukuhara, H., Nobukuni, T., Kanbe, T., Maruyama, T., Ghosh, H. P., Pletcher, M., Isomura, M., Onizuka, M., Kitamura, T., Sekiya, T., Reeves, R. H., and Murakami, Y. (2001) *Nat. Genet.* **27,** 427–430
2. Gomyo, H., Arai, Y., Tanigami, A., Murakami, Y., Hattori, M., Hosoda, F., Arai, K., Aikawa, Y., Tsuda, H., Hirohashi, S., Asakawa, S., Shimizu, N., Soeda, E., Sakaki, Y., and Ohki, M. (1999) *Genomics* **62,** 139–146
3. Urase, K., Soyama, A., Fujita, E., and Momoi, T. (2001) *Neuroreport* **12,** 3217–3221
4. Wakayama, T., Ohashi, K., Mizuno, K., and Iseki, S. (2001) *Mol. Reprod. Dev.* **60,** 158–164
5. Biederer, T., Sara, Y., Mozhayeva, M., Atasoy, D., Liu, X., Kavalali, E. T., and Sudhof, T. C. (2002) *Science* **297,** 1525–1531
6. Shingai, T., Ikeda, W., Kakunaga, S., Morimoto, K., Takekuni, K., Itoh, S., Satoh, K., Takeuchi, M., Imai, T., Monden, M., and Takai, Y. (2003) *J. Biol. Chem.* **278,** 35421–35427
7. Masuda, M., Yageta, M., Fukuhara, H., Kuramochi, M., Maruyama, T., Nomoto, A., and Murakami, Y. (2002) *J. Biol. Chem.* **277,** 31014–31019
8. Sasaki, H., Nishikata, I., Shiraga, T., Akamatsu, E., Fukami, T., Hidaka, T., Kubuki, Y., Okayama, A., Hamada, K., Okabe, H., Murakami, Y., Tsubouchi, H., and Morishita, K. (2005) *Blood* **105,** 1204–1213
9. Yasunaga, J., and Matsuoka, M. (2007) *Rev. Med. Virol.* **17,** 301–311
10. Tajima, K. (1990) *Int. J. Cancer* **45,** 237–243
11. Yamada, Y., Tomonaga, M., Fukuda, H., Hanada, S., Utsunomiya, A., Tara, M., Sano, M., Ikeda, S., Takatsuki, K., Kozuru, M., Araki, K., Kawano, F., Niimi, M., Tobinai, K., Hotta, T., and Shimoyama, M. (2001) *Br. J. Haematol.* **113,** 375–382
12. Matsuoka, M. (2005) *Retrovirology* **2,** 27
13. Yoshie, O. (2005) *Leuk. Lymphoma* **46,** 185–190
14. Yageta, M., Kuramochi, M., Masuda, M., Fukami, T., Fukuhara, H., Maruyama, T., Shibuya, M., and Murakami, Y. (2002) *Cancer Res.* **62,** 5129–5133
15. Fukuhara, H., Masuda, M., Yageta, M., Fukami, T., Kuramochi, M., Maruyama, T., Kitamura, T., and Murakami, Y. (2003) *Oncogene* **22,** 6160–6165
16. Songyang, Z., Fanning, A. S., Fu, C., Xu, J., Marfatia, S. M., Chishti, A. H., Crompton, A., Chan, A. C., Anderson, J. M., and Cantley, L. C. (1997) *Science* **275,** 73–77
17. Sheng, M., and Sala, C. (2001) *Annu. Rev. Neurosci.* **24,** 1–29

18. Boxus, M., Twizere, J. C., Legros, S., Dewulf, J. F., Kettmann, R., and Willems, L. (2008) *Retrovirology* 5, 76

19. Ishioka, K., Higuchi, M., Takahashi, M., Yoshida, S., Oie, M., Tanaka, Y., Takahashi, S., Xie, L., Green, P. L., and Fujii, M. (2006) *Retrovirology* 3, 71

20. Habets, G. G., Scholtes, E. H., Zuydgeest, D., van der Kammen, R. A., Stam, J. C., Berns, A., and Collard, J. G. (1994) *Cell* 77, 537–549

21. Michiels, F., Habets, G. G., Stam, J. C., van der Kammen, R. A., and Collard, J. G. (1995) *Nature* 375, 338–340

22. Ridley, A. J. (2006) *Trends Cell Biol.* 16, 522–529

23. Burridge, K., and Wennerberg, K. (2004) *Cell* 116, 167–179

24. Malliri, A., and Collard, J. G. (2003) *Curr. Opin. Cell Biol.* 15, 583–589

25. Garcia-Mata, R., and Burridge, K. (2007) *Trends Cell Biol.* 17, 36–43

26. Hoshino, H., Esumi, H., Miwa, M., Shimoyama, M., Minato, K., Tobinai, K., Hirose, M., Watanabe, S., Inada, N., Kinoshita, K., Kamihira, S., Ichimaru, M., and Sugimura, T. (1983) *Proc. Natl. Acad. Sci. U.S.A.* 80, 6061–6065

27. Wakayama, T., Koami, H., Ariga, H., Kobayashi, D., Sai, Y., Tsuji, A., Yamamoto, M., and Iseki, S. (2003) *Biol. Reprod.* 68, 1755–1763

28. Mao, X., Seidlitz, E., Ghosh, K., Murakami, Y., and Ghosh, H. P. (2003) *Cancer Res.* 63, 7979–7985

29. Furuno, T., Ito, A., Koma, Y., Watabe, K., Yokozaki, H., Bienenstock, J., Nakanishi, M., and Kitamura, Y. (2005) *J. Immunol.* 174, 6934–6942

30. Masuda, M., Kikuchi, S., Maruyama, T., Sakurai-Yageta, M., Williams, Y. N., Ghosh, H. P., and Murakami, Y. (2005) *J. Biol. Chem.* 280, 42164–42171

31. Ito, A., Okada, M., Uchino, K., Wakayama, T., Koma, Y., Iseki, S., Tsubota, N., Okita, Y., and Kitamura, Y. (2003) *Lab. Invest.* 83, 1175–1183

32. Ito, A., Nishikawa, Y., Ohnuma, K., Ohnuma, I., Koma, Y., Sato, A., Enomoto, K., Tsujimura, T., and Yokozaki, H. (2007) *Hepatology* 45, 684–694

33. Murakami, Y. (2005) *Cancer Sci.* 96, 543–552

34. Mertens, A. E., Roovers, R. C., and Collard, J. G. (2003) *FEBS Lett.* 546, 11–16

35. Sanchez-Madrid, F., and del Pozo, M. A. (1999) *EMBO J.* 18, 501–511

36. Gerard, A., Mertens, A. E., van der Kammen, R. A., and Collard, J. G. (2007) *J. Cell Biol.* 176, 863–875

37. Michiels, F., Stam, J. C., Hordijk, P. L., van der Kammen, R. A., Ruuls-Van Stalle, L., Feltkamp, C. A., and Collard, J. G. (1997) *J. Cell Biol.* 137, 387–398

38. Ceccarelli, D. F., Blasutig, I. M., Goudreault, M., Li, Z., Ruston, J., Pawson, T., and Sicheri, F. (2007) *J. Biol. Chem.* 282, 13864–13874

39. Minard, M. E., Kim, L. S., Price, J. E., and Gallick, G. E. (2004) *Breast Cancer Res. Treat* 84, 21–32

40. Stam, J. C., Michiels, F., van der Kammen, R. A., Moolenaar, W. H., and Collard, J. G. (1998) *EMBO J.* 17, 4066–4074

41. Malliri, A., van der Kammen, R. A., Clark, K., van der Valk, M., Michiels, F., and Collard, J. G. (2002) *Nature* 417, 867–871

42. Engers, R., Zwaka, T. P., Gohr, L., Weber, A., Gerharz, C. D., and Gabbert, H. E. (2000) *Int. J. Cancer* 88, 369–376

43. Hordijk, P. L., ten Klooster, J. P., van der Kammen, R. A., Michiels, F., Oomen, L. C., and Collard, J. G. (1997) *Science* 278, 1464–1466

44. Fogel, A. I., Akins, M. R., Krupp, A. J., Stagi, M., Stein, V., and Biederer, T. (2007) *J. Neurosci.* 27, 12516–12530

45. Galibert, L., Diemer, G. S., Liu, Z., Johnson, R. S., Smith, J. L., Walzer, T., Comeau, M. R., Rauch, C. T., Wolfson, M. F., Sorensen, R. A., Van der Vuurst de Vries, A. R., Branstetter, D. G., Koelling, R. M., Scholler, J., Fanslow, W. C., Baum, P. R., Derry, J. M., and Yan, W. (2005) *J. Biol. Chem.* 280, 21955–21964

46. Boles, K. S., Barchet, W., Diacovo, T., Cella, M., and Colonna, M. (2005) *Blood* 106, 779–786

47. Arase, N., Takeuchi, A., Unno, M., Hirano, S., Yokosuka, T., Arase, H., and Saito, T. (2005) *Int. Immunol.* 17, 1227–1237

48. Ito, A., Jippo, T., Wakayama, T., Morii, E., Koma, Y., Onda, H., Nojima, H., Iseki, S., and Kitamura, Y. (2003) *Blood* 101, 2601–2608

49. Ishida, T., and Ueda, R. (2006) *Cancer Sci.* 97, 1139–1146

50. Wu, K., Bottazzi, M. E., de la Fuente, C., Deng, L., Gitlin, S. D., Maddukuri, A., Dadgar, S., Li, H., Vertes, A., Pumfery, A., and Kashanchi, F. (2004) *J. Biol. Chem.* 279, 495–508

51. Matsuoka, M. (2003) *Oncogene* 22, 5131–5140

52. Dewan, M. Z., Takamatsu, N., Hidaka, T., Hatakeyama, K., Nakahata, S., Fujisawa, J., Katano, H., Yamamoto, N., and Morishita, K. (2008) *J. Virol.* 82, 11958–11963

Administration route-dependent induction of antitumor immunity by interferon-alpha gene transfer

Kenta Narumi,[1,3] Atsushi Kondoh,[1] Takeshi Udagawa,[1] Hidehiko Hara,[1] Naoko Goto,[1] Yoshinori Ikarashi,[1] Shumpei Ohnami,[2] Toshihide Okada,[3] Masakazu Yamagishi,[3] Teruhiko Yoshida[2] and Kazunori Aoki[1,4]

[1]Section for Studies on Host-Immune Response, [2]Genetics Division, National Cancer Center Research Institute, Tokyo; [3]Department of Internal Medicine, Kanazawa University Graduate School of Medical Science, Ishikawa, Japan

Type I interferon (IFN) protein is a cytokine with pleiotropic biological functions that include induction of apoptosis, inhibition of angiogenesis, and immunomodulation. We have demonstrated that intratumoral injection of an IFN-α-expressing adenovirus effectively induces cell death of cancer cells and elicits a systemic tumor-specific immunity in several animal models. On the other hand, reports demonstrated that an elevation of IFN in the serum following an intramuscular delivery of a vector is able to activate antitumor immunity. In this study, we compared the intratumoral and systemic routes of *IFN* gene transfer with regard to the effect and safety of the treatment. Intratumoral injection of an IFN-α adenovirus effectively activated tumor-responsive lymphocytes and caused tumor suppression not only in the gene-transduced tumors but also in distant tumors, which was more effective than the intravenous administration of the same vector. The expression of co-stimulatory molecules on CD11c$^+$ cells isolated from regional lymph nodes was enhanced by *IFN* gene transfer into the tumors. Systemic toxicity such as an elevation of hepatic enzymes was much lower in mice treated by intratumoral gene transfer than in those treated by systemic gene transfer. Our data suggest that the intratumoral route of the IFN vector is superior to intravenous administration, due to the effective induction of antitumor immunity and the lower toxicity. (*Cancer Sci* 2010; 101: 1686–1694)

Interferon-alpha (IFN-α) belongs to the group of type I interferons. It is produced by monocytes/macrophages, lymphoblastoid cells, fibroblasts, and plasmacytoid dendritic cells. Interferon-alpha (IFN-α) binds to the IFN-α receptor CD118, and the IFN receptor is coupled to a Janus-family tyrosine kinase, which phosphorylates signal-transducing activators of transcription (STATs), and STATs translocate to the nucleus where they activate the transcription of several different genes including the synthesis of host cell proteins that contribute to the inhibition of viral replication.[1] In addition to its antiviral activity, IFN-α exhibits several other antitumor functions: (i) direct inhibitory effects on tumor cell growth; (ii) radio and chemosensitizing effects; (iii) anti-angiogenic properties; and (iv) modulation of the immune system.[2–5] These features might be of special interest for use in cancer treatments.

Among the above antitumor properties, the direct inhibitory effects on tumor cell growth/functions and the interaction of IFN-α with chemotherapeutic drugs such as 5-FU have been of particular interest.[2,3] The cytokine has been used worldwide for treatment of a variety of cancers including chronic myelogeneous leukemia, melanoma, and renal cancer.[2,5] However, clinical experiences with IFN protein therapy for many other solid cancers have generally not been encouraging.[6] In the conventional regimen of IFN clinical trials, the recombinant IFN-α protein is systemically administered through subcutaneous or intramuscular routes. Since the protein is rapidly degraded in the blood circulation and only a small portion of subcutaneously injected IFN-α can reach the target sites,[7] the overall limited therapeutic efficacy of treatments based on the IFN-α protein may reflect the inability to target the cytokine to the right place and at the right dose. Alternative delivery strategies are needed to achieve a safe and effective IFN delivery in a clinical setting. In fact, it was reported that gene- and cell-based delivery of type I IFNs into tumors suppressed growth of various cancers such as breast cancer, prostate cancer, renal cancer, hepatocellular carcinoma, basal cell carcinoma, bladder cancer, and leukemia.[8–13] We have also shown that a single injection of the recombinant IFN-α protein into a tumor did not result in the suppression of tumor growth, whereas an intratumoral injection of an IFN-α-expressing adenovirus effectively induced cell death of cancer cells and did suppress the growth of tumors including pancreatic, colon, and renal cancers.[14–17]

Type I IFNs were long thought to act mainly by suppressing tumor cell proliferation *in vivo*. However, more recently, it has been established that type I IFNs have important roles in regulating innate and adaptive arms of the immune system: up-regulation of major histocompatibility complex (*MHC*) class I gene, promotion of the priming and survival of T cells, enhancement of humoral immunity, increase of the cytotoxic activity of natural killer (NK) cells and CD8$^+$ T cells, and activation of dendritic cells (DCs).[4,5] We have also shown that in addition to the direct cytotoxicity in the injected site, intratumoral injection of the IFN-α adenovirus elicits a significant systemic tumor-specific immunity in several animal models.[15,16] On the other hand, it has been reported that an intramuscular delivery of the *IFN-α* gene exhibited inhibition of tumor growth and that CD8$^+$ T cells were required for the antitumor response,[18,19] suggesting that an elevation of the IFN-α level in the serum also activates the antitumor immunity. However, it has not been examined whether the high IFN-α level in the tumor and blood circulation effectively induces antitumor immunity. It is difficult to inject high amounts of the IFN-α adenovirus into the muscle of mice without a leakage of the vector into the blood circulation, which may result in a variety of serum IFN-α levels among mice injected with the same amounts of IFN-α vector. Therefore, in this study, the adenovirus was injected into the tail vein to express consistent IFN-α at a high sustained level in the serum, and the antitumor immunity and safety were compared between the intratumoral and systemic routes of *IFN* gene transfer.

---

[4]To whom correspondence should be addressed. E-mail: kaoki@ncc.go.jp

Materials and Methods

Tumor cell line and recombinant adenovirus vectors. CT26 and Renca are weakly immunogenic BALB/c-derived colon and renal cancer cell lines, respectively, which were obtained from the American Type Culture Collection (Rockville, MD, USA). CT26 and Renca cells were confirmed to express MHC class I molecules (H-2K^d and H-2D^d) by flow cytometry; however, the heterogeneous MHC expression was observed in the subcutaneous tumors (data not shown). Cells were maintained in RPMI containing 10% FBS, 2 mM L-glutamine, and 0.15% sodium bicarbonate (complete RPMI). The recombinant adenovirus vectors expressing mouse interferon-α (Ad-mIFN) or alkaline phosphatase (Ad-AP) were prepared as described.[15,20] The recombinant adenoviruses are based on the serotype 5 with a deletion of the entire E1 region and a part of the E3 region, and have the CAG promoter, which is a hybrid of the cytomegalovirus immediate early enhancer sequence and the chicken β-actin/rabbit β-globin promoter, in the deleted E1 region.[21] A cesium chloride-purified virus was desalted using a sterile Bio-Gel P-6 DG chromatography column (Econopac DG 10; BioRad, Hercules, CA, USA) and diluted for storage in a 13% glycerol/PBS solution. All viral preparations were free of the E1$^+$ adenovirus by PCR assay.[22]

***In vivo* tumor inoculation and *IFN-α* gene transfer.** Tumor cells were prepared in a total volume of 100 μL PBS (5 × 10^6 of Renca and 1 × 10^6 of CT26 cells) and injected subcutaneously into the leg of BALB/c mice (Charles River Japan, Kanagawa, Japan). When the subcutaneous tumor was established (~0.5 cm in diameter), 50 μL of Ad-mIFN or control vector (Ad-AP) was injected once into the tumors or into the tail vein. The injection of 1 × 10^8 PFU (plaque forming unit) of Ad-AP showed that 70–80% of the cells were stained in the entire CT26 tumors. The shortest (*r*) and longest (*l*) tumor diameters were measured and the tumor volume was determined as $r^2 \times l/2$.

To deplete NK cells before and during the treatment with *IFN-α* gene transfer, BALB/c nude mice (Charles River Japan) received intraperitoneal injections of 0.5 mg of anti-asialo GM1 antibody targeting NK cells (Wako Pure Chemical Industries, Tokyo, Japan). Administration of antibody started 2 days after the inoculation of CT26 cells, and the injection was repeated every 5–6 days throughout the entire experimental period. Flow cytometry showed that more than 80% of NK cells were depleted in the antibody-treated mice.

Reverse transcription–polymerase chain reaction (RT-PCR) and ELISA analyses of IFN-α expression. Subcutaneous tumors were collected 4 days after the intratumoral or intravenous injection of Ad-mIFN or Ad-AP in the CT26 tumor-bearing BALB/c mice. To examine the expression of the *IFN-α* gene in the tumors, RT-PCR amplification was carried out using total RNA in a 50 μL of the PCR mixture with the following primer sets: IFN-α upstream (5′-GATGGTTCTGGCTGTGATGAG-3′) and downstream (5′-GATGTTCAGGATCTGCTGGGT-3′) primers; β-actin upstream (5′-CCTCTATGCCAACACAGTGC-3′) and downstream (5′-ATACTCCTGCTTGCTGATCC-3′) primers. In total, 33 cycles (β-actin, 25 cycles) of the PCR were carried out at 94°C for 1 min, 60°C for 1 min, and 72°C for 2 min. The PCR products were electrophoresed on a 2% agarose gel. Interferon-alpha (IFN-α) concentration in the serum, tumor and organs was measured by enzyme-linked immunosorbent assay (ELISA; Immunotech, Marseille Cedex, France).

ELISpot assays. Interferon-gamma (IFN-γ) ELISpot kits (BD Bioscience, San Jose, CA, USA) were used according to the manufacturer's instructions. CT26 cells were inoculated into the BALB/c mice, and 7 days later 1 × 10^8 PFU of Ad-mIFN or Ad-AP was administered into the tumors or into the tail vein. Twenty days later, splenocytes were harvested from the mice, and the splenocytes (1 × 10^5) and mitomycin C (MMC)-treated

CT26 cells (1 × 10^4) were co-cultured for 20 h at 37°C in complete RPMI medium in 96-well plates pre-coated with antimouse IFN-γ antibody (BD Bioscience) in triplicate. After aspirating the cells away and washing the wells with de-ionized water, a biotinylated antimouse IFN-γ antibody (2 μg/mL) was added and incubated for 2 h at room temperature. After extensive washing, a streptavidin–horseradish peroxidase solution was added and incubated for 1 h at room temperature. Then, an aminoethyl carbazole substrate solution was added, and the plate was incubated for 15 min. Spots were counted under a stereomicroscope.

Flow cytometry of co-stimulatory molecules. The regional lymph nodes were collected from the CT26 tumor-bearing mice 10 days after the intratumoral or intravenous injection of Ad-mIFN or Ad-AP (1 × 10^8 PFU). The 1 × 10^6 of cells from the lymph nodes were incubated at 4°C for 30 min with phycoerythrin-conjugated hamster antimouse CD11c monoclonal antibody (HL3; IgG; BD Biosciences), FITC-conjugated rat antimouse CD40 monoclonal antibody (3/23; IgG; BD Biosciences), FITC-conjugated hamster antimouse CD80 monoclonal antibody (16-10A1; IgG; BD Biosciences), FITC-conjugated rat antimouse CD86 monoclonal antibody (GL1; IgG; BD Biosciences), or isotype control antibody (IgG), and then washed twice with PBS containing 2% BSA. Flow cytometry was carried out using a FACScan system (BD Bioscience).

Immunohistochemistry. Immunostaining was performed using the streptavidin–biotin–peroxidase complex techniques (Nichirei, Tokyo, Japan). Consecutive cryostat tissue sections (5 μm) were mounted on glass slides and fixed in 99.5% ethanol for 20 min. After blocking with normal rat serum, the sections were stained with rat antimouse CD4 and CD8 antibodies (BD Biosciences). The cryostat sections were also processed for the terminal deoxynucleotidyltransferase-mediated dUTP-digoxigenin nick-end-labeling (TUNEL) assay (Intergen Company, Purchase, NY, USA). Negative controls without primary antibodies were examined in all cases. The sections were counterstained with methylgreen.

Statistical analysis. Two-sided *t*-tests were used to validate the significance of the observed differences, which were considered statistically significant when $P < 0.05$.

Results

Distribution of interferon-α in various organs following intratumoral or intravenous administration of Ad-mIFN. To confirm the *in vivo* expression of the *IFN-α* gene, total RNA of CT26 subcutaneous tumors was subjected to an RT-PCR analysis of the gene 4 days after the intratumoral or intravenous injection of Ad-mIFN or control Ad-AP (1 × 10^8 PFU). Intratumoral *IFN-α* gene transfer yielded a significant level of IFN-α expression in the tumor, whereas the intravenous route did not show the IFN-α band there (Fig. 1a). The IFN-α expression was not detected in the tumor injected with Ad-AP (Fig. 1a).

To determine the kinetics of IFN-α expression in the serum, the IFN-α levels were measured 3, 4, 7, and 13 days after the intratumoral or intravenous injection of Ad-mIFN. In the mice treated by intratumoral *IFN-α* gene transfer, the cytokine was slightly elevated at Day 3 and returned to a base line by Day 4, whereas in the mice with the intravenous injection of Ad-mIFN the peak levels in the serum were observed at Day 3 and the expression continued for more than 13 days, demonstrating that the intravenous gene transfer leads to the sustained high IFN-α expression in the blood circulation (Fig. 1b).

Then, to examine the *in vivo* distribution of IFN-α expression, we inoculated CT26 cells into both legs of BALB/c mice, followed by adenovirus (1 × 10^8 PFU) injection either into the right tumors or into the tail veins. Three days later the IFN-α levels were measured in the serum, subcutaneous tumors, and
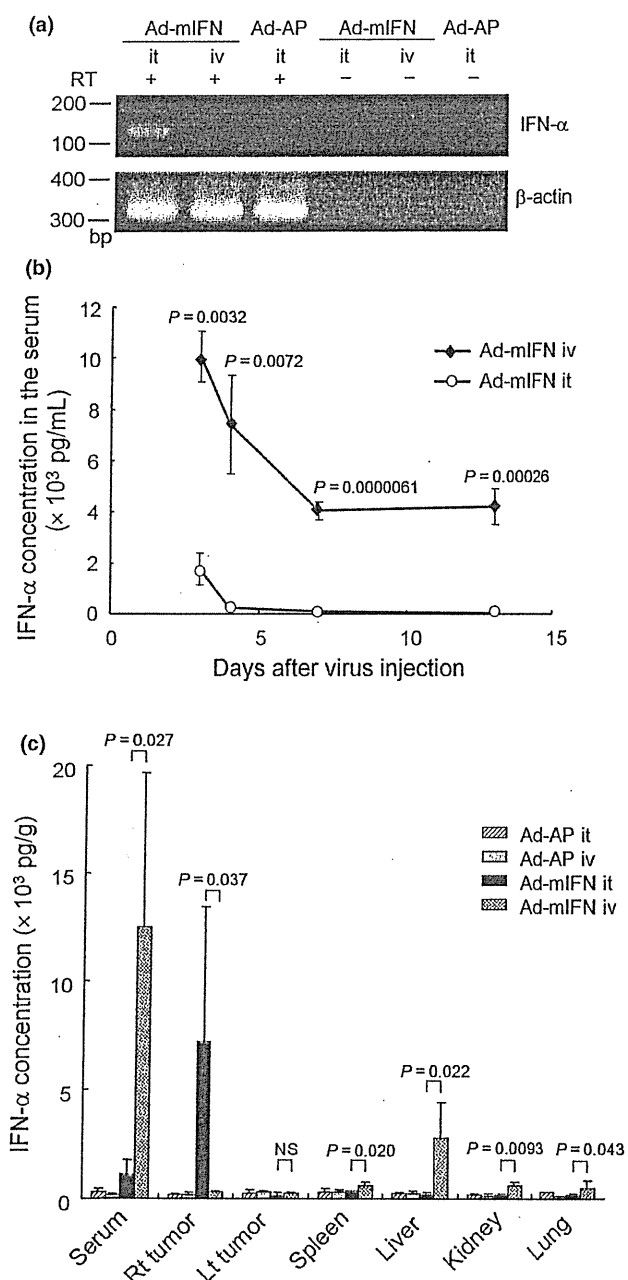
Fig. 1. Distribution of interferon-alpha (IFN-α) in the sera, subcutaneous tumors, and various organs. (a) Expression of *IFN-α* gene in subcutaneous tumors. The 1×10^8 PFU (plaque forming unit) of recombinant adenovirus vectors expressing mouse interferon-α (Ad-mIFN) or alkaline phosphatase (Ad-AP) was injected into the CT26 subcutaneous tumor or into the tail vein, and 4 days later the subcutaneous tumor was isolated, and IFN-α expression was examined by RT-PCR analysis. (b) Time course of IFN-α expression in the serum. The 1×10^8 PFU of Ad-mIFN was injected into the subcutaneous tumor or into the tail vein, and IFN-α concentration in the serum was measured by ELISA 3, 4, 7, and 13 days after the injection ($n = 4$). iv, intravenous injection; it, intratumoral injection. (c) Interferon-alpha (IFN-α) concentration in the sera, tumors, and organs. The 1×10^8 PFU of adenoviruses was injected into the subcutaneous tumor or into the tail vein, and 3 days later IFN-α concentration was measured ($n = 4$). Rt, right; Lt, left.

various organs such as the spleen, liver, kidney, and lung. In the mice treated by intratumoral *IFN-α* gene transfer, the serum showed a slight elevation of IFN-α, whereas its concentration

was highest in the right virus-injected tumor (Fig. 1c), which was approximately 10-fold higher than the serum as previously described.[14,15,17,23] In the mice treated by intravenous *IFN-α* gene transfer, the IFN-α level was significantly elevated in the serum and various organs including the liver but not in the subcutaneous tumors compared with the intratumoral *IFN-α* gene transfer (Fig. 1c). The IFN-α was not elevated in the serum, tumors, or organs in the mice that received the administration of Ad-AP.
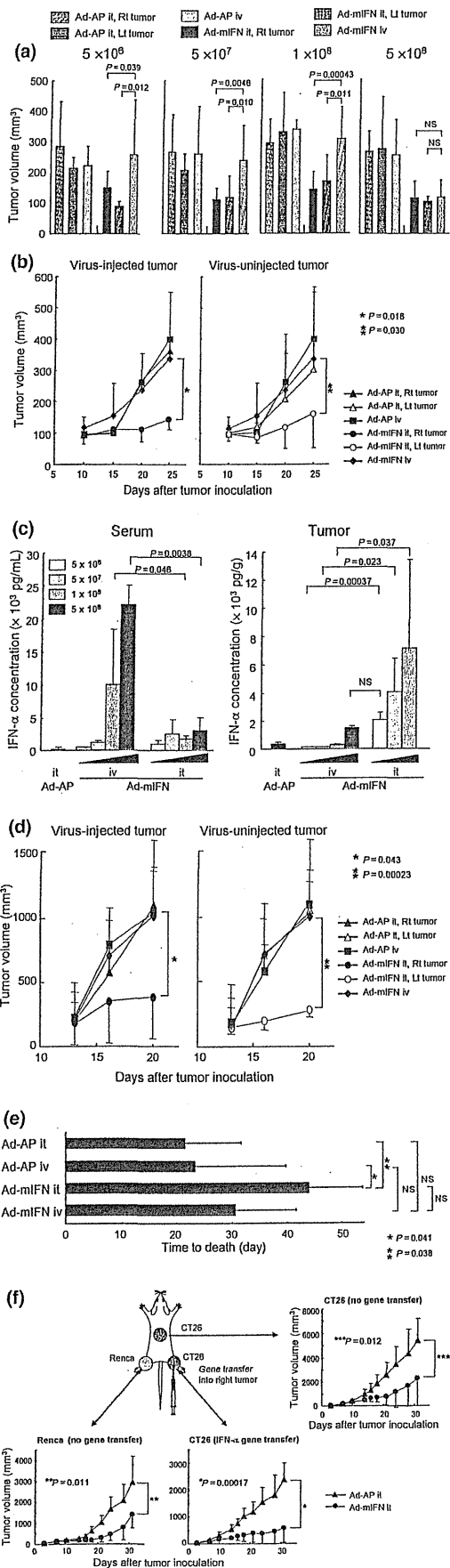
Antitumor effects of intratumoral and intravenous administration of Ad-mIFN. To examine the *in vivo* antitumor effect of the *IFN-α* gene transduction, various amounts (5×10^6, 5×10^7, 1×10^8, and 5×10^8 PFU) of adenoviruses were injected into right tumors or into the tail veins in mice with CT26 tumors on both legs. The intravenous injection of Ad-mIFN did not show a definite suppressive effect except at the highest dose examined (5×10^8 PFU), which resulted in tumor suppression comparable with that of the intratumoral injection (Fig. 2a). The intratumoral injection of Ad-mIFN showed remarkable tumor suppressive effects in not only the vector-injected right tumors but also in the vector-uninjected left tumors at all doses examined (Fig. 2a,b). Tumor volumes were not changed in the mice treated by intratumoral and intravenous injections of Ad-AP at any doses (Fig. 2a), which were similar to those in the no treatment group (data not shown).

To compare the IFN-α levels in the tumors with the antitumor effects, an IFN-α concentration was examined 3 days after the gene transfer. The IFN-α concentration in the tumors following the intratumoral gene transfer was elevated in a dose-dependent manner, and the levels were much higher than those for the intravenous injections at all doses (Fig. 2c). An intravenous injection of less than 1×10^8 PFU of Ad-mIFN did neither elevate the IFN-α concentration in the tumors nor suppress the tumor growth. By contrast, the intravenous injection of the high dose (5×10^8 PFU) resulted in 1522.2 pg/g of IFN-α in the tumors, which was close to that (2054.7 pg/g) after an intratumoral injection of low dose (5×10^6 PFU) of Ad-mIFN (Fig. 2c), and significantly suppressed tumor growth (Fig. 2a). The increase of the IFN-α level in the tumor might be related to induction of an effective antitumor immunity.

To confirm the antitumor activity of intratumoral *IFN-α* gene transfer in a different tumor cell line, 1×10^8 PFU of Ad-mIFN was injected into Renca tumor-bearing mice. The antitumor activity of an intratumoral injection was also evident against the renal cancer cells (Fig. 2d), and resulted in a statistically significant improvement in the survival of the treated mice as compared with the Ad-AP-injected animals (Fig. 2e).

Then, we inoculated CT26 cells on the right legs and on the backs and Renca cells on the left legs of BALB/c mice, and 1×10^8 PFU of Ad-mIFN was injected into CT26 tumors on the right legs. Interferon-alpha (*IFN-α*) gene transfer suppressed the growth of not only the right leg CT26 tumors but also the back CT26 tumors; and the growth of Renca tumors, which were not transduced with *IFN-α* gene, on the left legs was also significantly suppressed compared with the Ad-AP injection (Fig. 2f). Certain tumor-associated antigens (TAAs) might be shared by CT26 and Renca tumors. Alternatively, the activation of NK cells by the IFN-α expression may be responsible for this phenomenon as later described.

Cell-death induction and infiltration of CD4$^+$ and CD8$^+$ cells in the tumors. To examine whether the IFN-α expression induces cell death in the tumors, TUNEL assay was performed using tumors of mice treated by *IFN-α* gene transfer. The assay revealed massive cell death of cancer cells in Ad-mIFN-injected tumors as shown in our previous reports,[17] but TUNEL-positive cells were also recognized albeit relatively sparsely in the vector-uninjected tumors in the mice treated by intratumoral *IFN-α* gene transfer (Fig. 3a). The difference in numbers of

(a) 5 ×10⁶ 5 ×10⁷ 1 ×10⁸ 5 ×10⁸

(b) Virus-injected tumor   Virus-uninjected tumor

(c) Serum   Tumor

(d) Virus-injected tumor   Virus-uninjected tumor

(e)

(f)

Fig. 2. Intratumoral interferon-alpha (IFN-α) gene transfer induces a systemic antitumor effect. CT26 cells were inoculated in both legs in BALB/c mice, and 7 days later recombinant adenovirus vectors expressing mouse interferon-α (Ad-mIFN) or alkaline phosphatase (Ad-AP) was injected into the subcutaneous tumor on the right leg or into the tail vein. (a) Growth suppression of the CT26 subcutaneous tumors 20 days after the tumor inoculation. Various amounts (5×10^6, 5×10^7, 1×10^8, and 5×10^8 PFU [plaque forming unit]) of adenoviruses were injected, and 13 days after the virus injection tumor volume was measured ($n = 6$). In the mice treated by intratumoral injection of adenoviruses, tumor volumes on both legs were combined to calculate the average. (b) Time course of CT26 tumor growth following intratumoral IFN-α gene transfer. The 5×10^7 PFU of adenoviruses was injected, and tumor volume was measured at indicated days ($n = 6$). (c) Interferon-alpha (IFN-α) levels after the injection of various amounts of Ad-mIFN. Various amounts of Ad-mIFN were injected into the subcutaneous tumor or into the tail vein, and 3 days later IFN-α concentration was measured in the serum and tumor ($n = 3$). The IFN-α concentration in the tumors injected with 5×10^8 PFU of Ad-mIFN was 13895.3 ± 5916.1 pg/g. (d) Time course of Renca tumor growth. The 1×10^8 PFU of adenoviruses was injected, and tumor volume was measured at indicated days ($n = 4$). In the mice treated by intravenous injection of adenoviruses, tumor volumes for both legs were combined to calculate the average. (e) Survival of mice treated by intratumoral or intravenous injection of adenoviruses. The 1×10^8 PFU of adenoviruses was injected in the Renca tumor-bearing mice, and a time to death after tumor inoculation was assessed ($n = 6$). (f) Growth suppression of CT26 and Renca tumors. CT26 cells were inoculated on the right legs and on the backs and Renca cells were inoculated on the left legs in BALB/c mice, and then 1×10^8 PFU of Ad-mIFN was injected into the CT26 tumor on the right leg ($n = 6$).

TUNEL-positive cells is probably due to presence of the direct cell-death induction by the IFN-α expression in the injected but not uninjected tumors.

To determine whether the different therapeutic efficacies between the intratumoral and intravenous *IFN*-α gene transfer are associated with different T-cell responses, we analyzed the infiltration of CD4⁺ and CD8⁺ cells into the subcutaneous tumors by immunostaining 10 days after the vector injection. The intratumoral IFN-α expression significantly increased the infiltration of CD4⁺ and CD8⁺ T cells in the tumors on both legs, compared to the intravenous administration of Ad-mIFN (Fig. 3a,b). No increases of those cells were observed in the Ad-AP-treated mice. The infiltrated immune cells could induce an antitumor effect against tumors, in particular at distant sites.

Natural killer (NK) cells also play a role in antitumor effect of intratumoral Ad-mIFN administration. It has been reported that IFN-α enhances the activity of NK cells[4] in addition to the activation of cytotoxic T lymphocyte. To determine whether the absence of T cells abrogates IFN-α-mediated therapeutic efficacy, we inoculated CT26 cells in both legs of BALB/c nude mice, and then injected 5×10^7 PFU of Ad-mIFN into the tumor on the right leg or into the tail vein. The intravenous *IFN*-α gene transfer showed modest tumor growth inhibition compared with the Ad-AP injection, whereas a marked suppression of both vector-injected and vector-uninjected tumors was observed after intratumoral *IFN*-α gene transfer (Fig. 4a). The depletion of NK cells with anti-asialo GM1 antibody cancelled the antitumor effect of vector-uninjected tumors on the left legs almost completely, whereas significant growth suppression was still recognized in the Ad-mIFN-injected tumors on the right legs (Fig. 4b), possibly due to the direct cell-death induction by IFN-α expression. The results suggest that the NK cells in the regional tumor are activated by the IFN-α expression and contribute to systemic antitumor immunity, which is consistent with our previous report.[15] Interestingly, the intravenous injection of 5×10^7 PFU of Ad-mIFN suppressed the tumor growth in immune-deficient nude mice (Fig. 4a) but not in immune-competent mice (Fig. 2b). The difference may be explained by the

Narumi *et al.*

fact that activity of NK cells is more elevated in nude mice compared with immune-competent mice, and by the possibility that an increase of the serum IFN-α concentration effectively enhances the cytotoxicity of the NK cells more than that of T cells. Although it could be due to augmented IFN-α production since nude mice have less ability to exclude adenovirus, the serum IFN-α concentration of nude mice 4 days after the intravenous injection of Ad-mIFN (1×10^8 PFU) was 5444.1 ± 244.7 pg/mL, which was not significantly different from the value (7402.9 ± 1912.1 pg/mL) of BALB/c mice (Fig. 1b).

Expansion of tumor-responsive lymphocytes after intratumoral *IFN-α* gene transfer. To examine the expansion of tumor-responsive lymphocytes after intratumoral or intravenous *IFN-α* gene transfer in immune-competent BALB/c mice, the splenocytes were harvested 20 days after the vector administration, and stimulated with MMC-treated CT26 cells or syngeneic lymphocytes. ELISpot assay showed that the intravenous *IFN-α* gene transfer slightly increased the number of IFN-γ-secreting cells in response to CT26 cells compared with the control Ad-AP injection, and that the intratumoral *IFN-α* gene transfer resulted in a significantly higher number of IFN-γ-positive spots than the intavenous injection (Fig. 5a, left), suggesting that the IFN-α expression in the tumor effectively expanded tumor-responsive immune cells including cytotoxic T cells and NK cells. Spot numbers of lymphocytes from CT26 tumor-bearing mice with no treatment were similar to those with the Ad-AP injection (data not shown). Intratumoral *IFN-α* gene transfer did not significantly change the number of IFN-γ-positive spots for syngeneic lymphocytes, whereas the intravenous route of the same vector increased the number of spots for lymphocytes (Fig. 5a, right). The elevation of the IFN-α concentration in the serum may enhance the lymphocyte reactivity nonspecifically.

Antigen presentation by DCs isolated from vector-injected tumors. After antigen capture, and in response to inflammatory stimuli, DCs mature and migrate to lymph nodes to initiate immunity. To verify whether the expression of IFN-α in the tumors augments the maturation of the antigen presenting cells, we isolated CD11c^{+} cells from the regional lymph nodes of tumor-bearing mice treated with adenoviruses, and examined the expression of co-stimulatory molecules on the cells. Flow cytometry showed that the frequency of CD11c^{+} cell per lymphocyte increased and the expressions of CD40, CD80, and CD86 were up-regulated in CD11c^{+} cells isolated from the mice treated by intratumoral *IFN-α* gene transfer. The expression of CD86 in CD11c^{+} cells after intravenous injections of Ad-mIFN was slightly increased compared with the Ad-AP-injected mice (Fig. 5b). The results indicate that IFN-α expression in the tumor effectively enhances the maturation of CD11c^{+} cells in the regional lymph nodes more than the high systemic level of IFN-α does.

Then, to examine whether the enhanced expression of co-stimulatory molecules on DCs is associated with antigen presentation, CD4^{+} T cells derived from the spleen of CT26 tumor-bearing control mice were co-cultured for 3 days with the CD11c^{+} cells isolated from the tumors in the vector-treated mice and MMC-treated CT26 cells. The production of IFN-γ protein from the isolated CD11c^{+} cells *per se* was minimal in the *in vitro* culture (data not shown). ELISpot analysis showed that a primary culture with CD11c^{+} cells isolated from the tumors treated by Ad-mIFN resulted in a higher number of IFN-γ-secreting CD4^{+} T cells than cultures with CD11c^{+} cells isolated from tumors in the intravenously Ad-mIFN-, intratumorally Ad-AP-, and intravenously Ad-AP-injected mice (Fig. 5c), demonstrating that the antigen presentation capacity of DCs was significantly enhanced by IFN-α expression in the tumor.
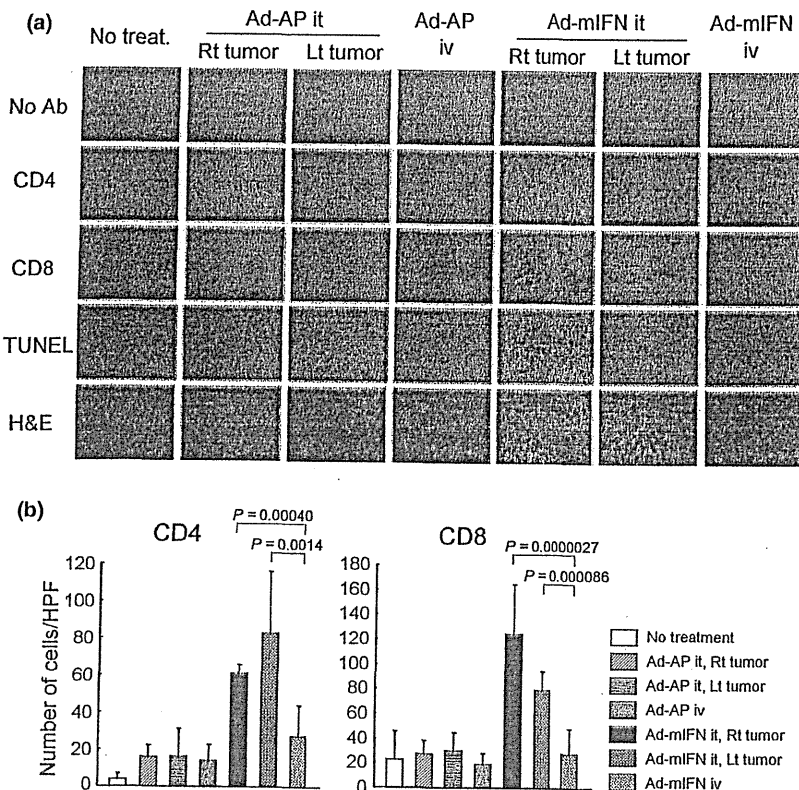

Fig. 3. Infiltration of CD4^{+} and CD8^{+} T cells into the tumors. (a) Immunohistochemical staining of CT26 tumors. Ten days after the administration of adenoviruses, the fresh frozen sections of subcutaneous tumors were processed for immunohistochemistry with anti-CD4 and anti-CD8 antibodies, and also processed for TUNEL staining (×400). Ab, antibody; H&E, hematoxylin–eosin. (b) Number of CD4^{+} and CD8^{+} T cells in CT26 tumors. Positive cells were counted in 10 representative high power view fields (HPF, ×400) under microscope.

(a)

(b) Virus-injected tumor   Virus-uninjected tumor

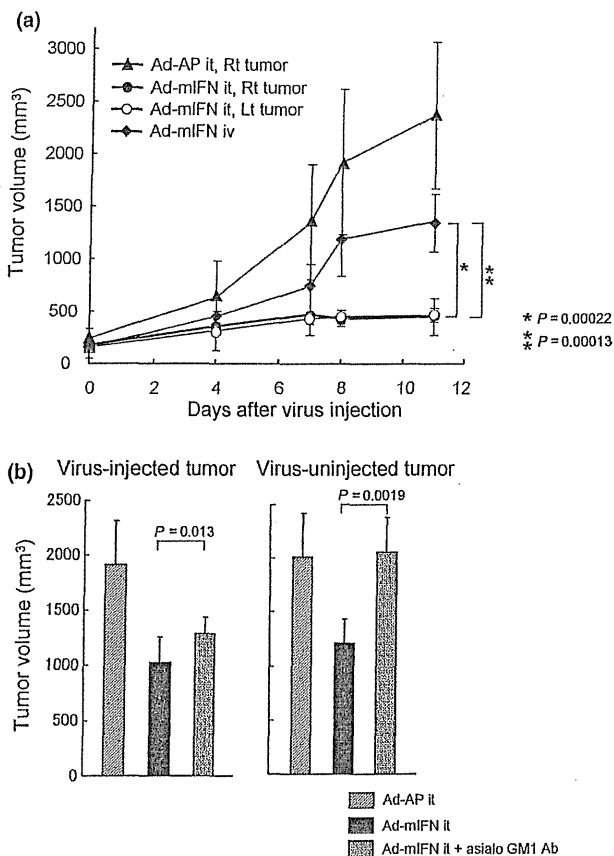Ad-AP it
Ad-mIFN it
Ad-mIFN it + asialo GM1 Ab

Fig. 4. Suppression of CT26 tumors in nude mice. (a) The CT26 cells were inoculated on both legs of BALB/c nude mice, and 7 days later 5 × 10⁷ PFU (plaque forming unit) of recombinant adenovirus vectors expressing mouse interferon-α (Ad-mIFN) or alkaline phosphatase (Ad-AP) was injected into the right tumor or into the tail vein. (b) BALB/c nude mice were treated with anti-asialo GM1 antibody, and the CT26 tumors were injected with 5 × 10⁷ PFU of Ad-mIFN ($n = 7$). Tumor volumes 10 days after interferon-alpha ($IFN-\alpha$) gene transfer are presented.

Fig. 5. Activation of antigen-presenting cells isolated from the mice treated by interferon-alpha ($IFN-\alpha$) gene transfer. (a) Expansion of tumor-responsive T cells after intratumoral injection of recombinant adenovirus vector expressing mouse interferon-α (Ad-mIFN). ELISpot assay of interferon-gamma (IFN-γ)-producing cells was performed in response to stimulation of CT26 cells. Ad-mIFN or recombinant adenovirus vector expressing alkaline phosphatase (Ad-AP) was injected into the CT26 tumor or into the tail vein and 20 days later splenocytes were co-cultured with CT26 cells or lymphocytes, and stained with biotinylated antimouse IFN-γ antibody to detect captured IFN-γ ($n = 3$). Lymphocytes were isolated from the spleen of a naïve BALB/c mouse. (b) Expression of co-stimulatory molecules on CD11c⁺ cells. Flow cytometry of CD40, CD80, and CD86 expressions was performed on CD11c⁺ cells isolated from regional lymph nodes of the mice treated by intratumoral or intravenous injection of Ad-mIFN or Ad-AP ($n = 3$–4). The frequency of CD11c⁺ cells (upper left) per lymphocytes, and CD40⁺ (upper right), CD80⁺ (lower left), and CD86⁺ (lower right) cells per CD11c⁺ cells are presented. (c) Number of IFN-γ-producing cells by the stimulation of CD11c⁺ cells. CD11c⁺ cells were isolated from the tumors of treated mice. CD4⁺ T cells were isolated from the spleens of CT26 tumor-bearing mice, and co-cultured with CT26 cells and the isolated CD11c⁺ cells for 3 days, and then the number of IFN-γ-producing CD4⁺ T cells was counted. AP-CD11c⁺, CD11c⁺ cells isolated from tumors in mice treated by Ad-AP. mIFN-CD11c⁺, CD11c⁺ cells isolated from tumors in mice treated by Ad-mIFN.

Lower systemic toxicity after intratumoral injection of Ad-mIFN. To compare the toxicity between the administration routes of the IFN-α vector, different doses (1×10^8, 5×10^8, 1×10^9, and 3×10^9 PFU) of Ad-mIFN or Ad-AP were injected into the subcutaneous tumors or into the tail veins of mice. All three mice treated by intravenous injection of 3×10^9 PFU of Ad-mIFN died within 4 days after the vector administration, whereas all the mice treated by the intratumoral injection of the same amount of Ad-mIFN survived and appeared healthy up to
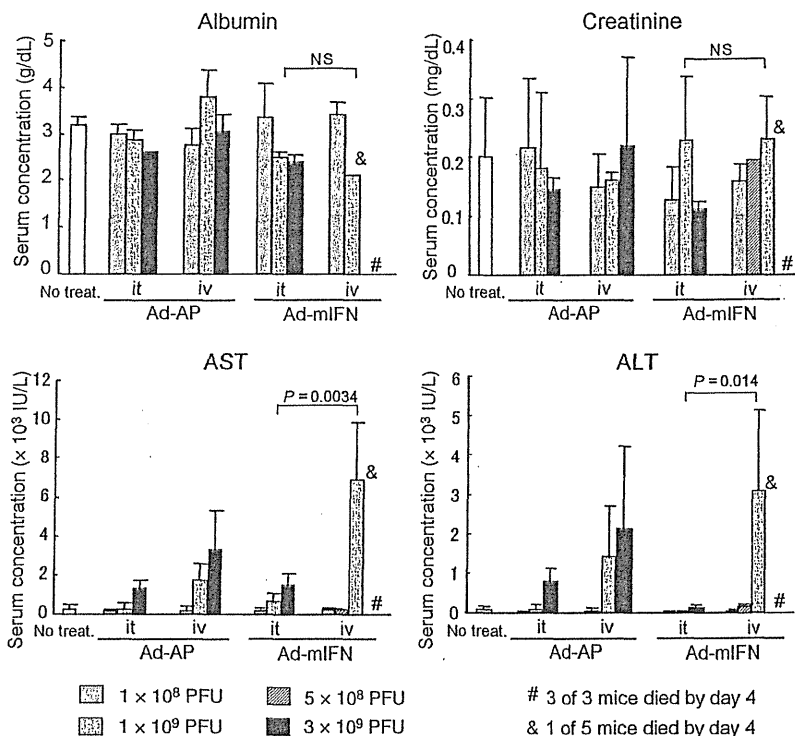
(a)

(b)

(c)

Narumi *et al.*
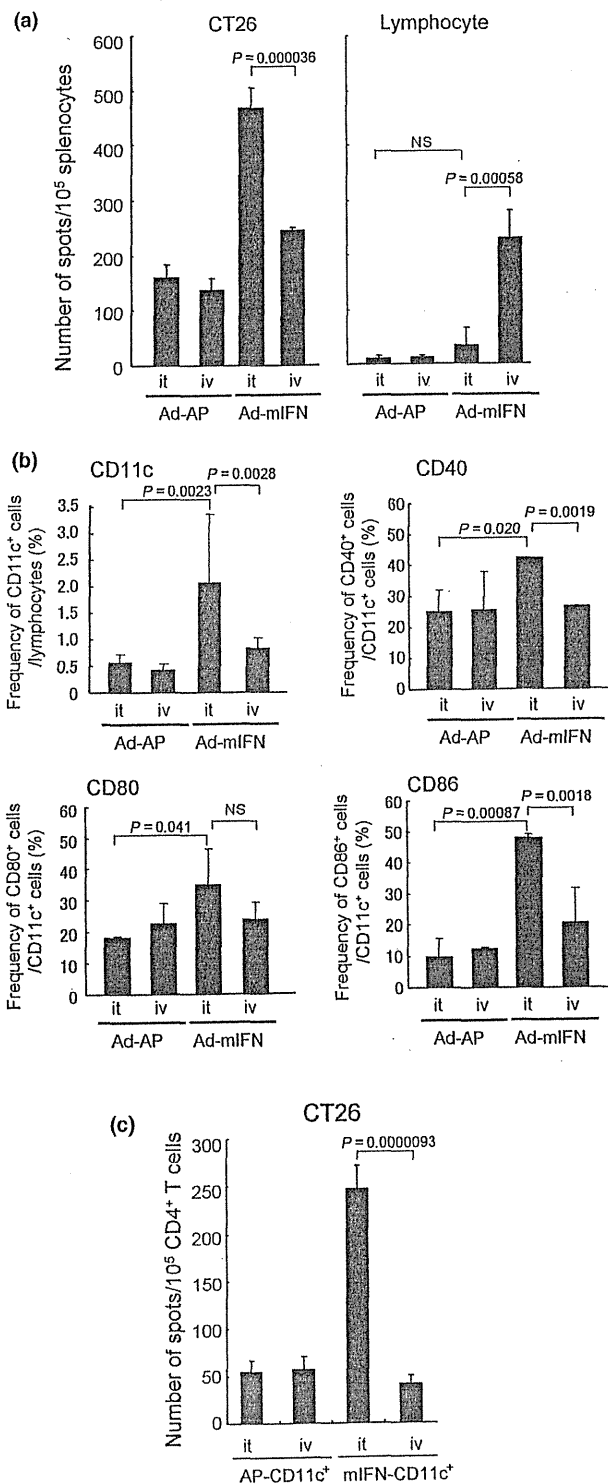
Fig. 6. Elevation of hepatic enzymes after intravenous injection of recombinant adenovirus vector expressing mouse interferon-α (Ad-mIFN). Different doses (1×10^8, 5×10^8, 1×10^9, and 3×10^9 PFU) of Ad-mIFN or recombinant adenovirus vector expressing alkaline phosphatase (Ad-AP) were injected into the subcutaneous tumor or into the tail vein. Five days later the selected blood chemistries (albumin, creatinine, aspartate aminotransferase (AST), and alanine aminotransferase (ALT)) were examined ($n = 3$).

Legend:
1×10^8 PFU 5×10^8 PFU
1×10^9 PFU 3×10^9 PFU
\# 3 of 3 mice died by day 4
& 1 of 5 mice died by day 4

5 days, when the mice were sacrificed to evaluate serum enzyme values. In the mice that received the intravenous *IFN-α* gene transfer, the injection of 1×10^9 PFU significantly elevated the aspartate aminotransferase (AST) and alanine aminotransferase (ALT) levels (more than 100-fold higher than the average value in normal mice) in the serum, and the injection of 5×10^8 PFU slightly elevated the ALT level (5.7-fold higher than the average value) (Fig. 6). Although the intratumoral injection of Ad-mIFN slightly increased the AST level in a dose-dependent manner, the values were similar to the intratumoral injection of Ad-AP, confirming the lower systemic toxicity after the intratumoral *IFN-α* gene transfer. Regarding albumin and creatinine, there was no significant difference among the treated mice (Fig. 6).

Discussion

It has been reported that the modes of antitumor responses of *IFN-α* gene therapy manifested three aspects: direct antiproliferative effect,[1] stimulation of antitumor immunity,[4] and anti-angiogenesis activity.[24] Our previous reports also showed that an intratumoral *IFN-α* gene transfer induces a marked regional antitumor effect and an effective systemic immunity.[15,16] This immunity was not attributable to the elevated level of the IFN-α in the systemic circulation, because we found a little leakage of the cytokine following the intratumoral injection of the IFN-expressing adenovirus.[15,17] On the other hand, the elevation of the systemic IFN-α level after intramuscular delivery of the *IFN-α* gene was reported to exhibit an inhibition of tumor growth by the infiltration of CD8⁺ T cells.[18,19] Therefore, in this study, we compared the induction of systemic antitumor immunity by a high IFN-α level in the tumor and blood circulation. The antitumor effects and general toxicities in the mice treated by intratumoral or intravenous injection of Ad-mIFN at various doses are summarized in Table 1. The tumor growth suppression was recognized at the lowest dose (5×10^6 PFU) and the toxicity was not observed at levels of less than 1×10^9 PFU in the mice treated by the intratumoral *IFN-α* gene

Table 1. Summary of antitumor effects and toxicities by intratumoral and intravenous injection of Ad-mIFN at various doses

Route	Dose	Antitumor effect	Toxicity
Intratumoral injection	5×10^6	++	NE
	5×10^7	++	NE
	1×10^8	++	–
	5×10^8	++	NE
	1×10^9	NE	–
	3×10^9	NE	+
Intravenous injection	5×10^6	–	NE
	5×10^7	–	NE
	1×10^8	–	–
	5×10^8	++	+
	1×10^9	NE	+++
	3×10^9	NE	+++

Antitumor effect was evaluated on the basis of tumor growth compared with recombinant adenovirus vector expressing alkaline phosphatase (Ad-AP)-injected tumors: +, >70%; ++, 30–70%; +++, <30%. Toxicity was evaluated on the basis of the elevation of aspartate aminotransferase (AST) or alanine aminotransferase (ALT) values compared with average in normal mice: +, >5-fold elevation; ++, 5–100-fold elevation; +++, >100-fold elevation or death. Ad-mIFN, recombinant adenovirus vector expressing mouse interferon-α; NE, not evaluated.

transfer, whereas the antitumor effect only appeared at 5×10^8 PFU, and hepatic toxicity was observed at the 5×10^8 PFU level, in the mice treated by intravenous gene transfer. The results suggested that the intratumoral route of IFN vector is superior to intravenous administration, due to the effective induction of an antitumor immunity and the lower toxicity.

The underlying mechanism of the antitumor immunity induced by *IFN-α* gene transfer is not fully understood. In this study, we noticed the role of IFN-α in the maturation and function of DCs. Dendritic cells (DCs) are antigen-presenting cells specialized to induce T-cell responses against cells exposing

foreign peptides including TAAs, and DCs show an effective cross-priming with antigens from apoptotic tumor cells.[25,26] As shown in Figure 3a and our previous report,[17] a high IFN-α level after intratumoral injection of an adenovirus vector induced apoptotic cell death in CT26 subcutaneous tumors, and abundant apoptosis induced by intratumoral IFN-α expression may expose TAAs in large quantity and enhance the uptake of released TAAs by DCs. Moreover, recent data have shown that type I IFN itself can act as an important signal for differentiation and maturation of DC: DCs generated after a few days of treatment with IFN-α showed the mature phonotype.[4,27] It is known that maturation of DCs is associated with up-regulation of the co-stimulatory molecules, and enhancement of their antigen-presenting function.[28] In this study also, the CD11+ cells isolated from regional sites of mice treated by intratumoral IFN gene transfer showed up-regulations of CD40, CD80, and CD86 (Fig. 5b) and the enhancement of antigen-presentation capacity (Fig. 5c). Finally, TAA-specific T cells activated by DCs could efficiently infiltrate into the CT26 tumors, leading to antitumor effect. Therefore, the effective apoptosis induction and direct immunomodulatory effect of IFN-α on DCs may contribute to the observed augmentation of the tumor specific immunity.

Intravenous administration of an adenovirus results in gene delivery primarily to the liver.[29,30] We previously reported a significant production of IFN-α in the liver after an intravenous injection of 1×10^7 of an IFN-α-expressing adenovirus vector in the dimethylnitrosamine-induced cirrhotic rat, but no IFN-α was detected in the serum.[31] The transgene expression was mainly observed in the fibrous septa but not in hepatocytes in a cirrhotic liver, whereas it was detected in septa as well as in hepatocytes in the normal rats.[31] In this study, we intravenously injected 1×10^8 PFU of Ad-mIFN to examine the biodistribution of IFN-α expression in various mice organs (Fig. 1c). The difference in the amount of the injected virus and the

histopathology of the liver may be the reason that high IFN-α levels were sustained in the serum in this study.

It is well known that a systemic administration of IFN-α protein often induces severe adverse effects such as flu-like symptoms, leucopenia, liver dysfunction, and mental depression.[32] With respect to the safety of a local IFN-α gene therapy, it is noteworthy that the intratumoral IFN-α gene transfer showed very limited general toxicity such as an elevation of hepatic enzymes, since the IFN-α concentration in the serum was approximately 6–68-fold lower in the intratumorally Ad-mIFN-injected mice compared with the intravenously Ad-mIFN-injected mice (Fig. 1b). The apparent difference in the IFN-α concentration between the tumor and serum is an important finding especially from the viewpoint of safety of local IFN-α gene therapy. As one of the reasons for a little leakage of the IFN-α protein from the tumors into blood circulation, we recently reported that extracellular matrix proteins such as fibronectin in tumors directly interact with IFN-α and retain the cytokine.[23]

In summary, our preclinical study suggests that a regional adenovirus-mediated gene transfer of IFN-α is one of the promising new approaches to cancer. The strategy may deserve an evaluation in a future clinical trial for intractable cancer.

Acknowledgments

References

1 Caraglia M, Marra M, Pelaia G et al. Alpha-interferon and its effects on signal transduction pathways. J Cell Physiol 2005; 202: 323–35.
2 Pfeffer LM, Dinarello CA, Herberman RB et al. Biological properties of recombinant alpha-interferons: 40th anniversary of the discovery of interferons. Cancer Res 1998; 58: 2489–99.
3 Gutterman JU. Cytokine therapeutics: lessons from interferon alpha. Proc Natl Acad Sci USA 1994; 91: 1198–205.
4 Santini SM, Lapenta C, Santodonato L, D'Agostino G, Belardelli F, Ferrantini M. IFN-alpha in the generation of dendritic cells for cancer immunotherapy. Handb Exp Pharmacol 2009; 188: 295–317.
5 Ferrantini M, Capone I, Belardelli F. Dendritic cells and cytokines in immune rejection of cancer. Cytokine Growth Factor Rev 2008; 19: 93–107.
6 Einhorn S, Grander D. Why do so many cancer patients fail to respond to interferon therapy? J Interferon Cytokine Res 1996; 16: 275–81.
7 Salmon P, Le Cotonnec JY, Galazka A, Abdul-Ahad A, Darragh A. Pharmacokinetics and pharmacodynamics of recombinant human interferon-beta in healthy male volunteers. J Interferon Cytokine Res 1996; 16: 759–64.
8 Zhang JF, Hu C, Geng Y et al. Treatment of a human breast cancer xenograft with an adenovirus vector containing an interferon gene results in rapid regression due to viral oncolysis and gene therapy. Proc Natl Acad Sci USA 1996; 93: 4513–8.
9 Hottiger MO, Dam TN, Nickoloff BJ, Johnson TM, Nabel GJ. Liposome-mediated gene transfer into human basal cell carcinoma. Gene Ther 1999; 6: 1929–35.
10 Ahmed CM, Wills KN, Sugarman BJ et al. Selective expression of nonsecreted interferon by an adenoviral vector confers antiproliferative and antiviral properties and causes reduction of tumor growth in nude mice. J Interferon Cytokine Res 2001; 21: 399–408.
11 Benedict WF, Tao Z, Kim CS et al. Intravesical Ad-IFNalpha causes marked regression of human bladder cancer growing orthotopically in nude mice and overcomes resistance to IFN-alpha protein. Mol Ther 2004; 10: 525–32.
12 Studeny M, Marini FC, Dembinski JL et al. Mesenchymal stem cells: potential precursors for tumor stroma and targeted-delivery vehicles for anticancer agents. J Natl Cancer Inst 2004; 96: 1593–603.

13 De Palma M, Mazzieri R, Politi LS et al. Tumor-targeted interferon-alpha delivery by Tie2-expressing monocytes inhibits tumor growth and metastasis. Cancer Cell 2008; 14: 299–311.
14 Hatanaka K, Suzuki K, Miura Y et al. Interferon-alpha and antisense K-ras RNA combination gene therapy against pancreatic cancer. J Gene Med 2004; 6: 1139.
15 Ohashi M, Yoshida K, Kushida M et al. Adenovirus-mediated interferon alpha gene transfer induces regional direct cytotoxicity and possible systemic immunity against pancreatic cancer. Br J Cancer 2005; 93: 441–9.
16 Hara H, Kobayashi A, Yoshida K et al. Local interferon-alpha gene therapy elicits systemic immunity in a syngeneic pancreatic cancer model in hamster. Cancer Sci 2007; 98: 455–63.
17 Hara H, Kobayashi A, Narumi K et al. Intratumoral interferon-alpha gene transfer enhances tumor immunity after allogeneic hematopoietic stem cell transplantation. Cancer Immunol Immunother 2009; 58: 1007–21.
18 Horton HM, Anderson D, Hernandez P, Barnhart KM, Norman JA, Parker SE. A gene therapy for cancer using intramuscular injection of plasmid DNA encoding interferon alpha. Proc Natl Acad Sci USA 1999; 96: 1553–8.
19 Li S, Zhang X, Xia X et al. Intramuscular electroporation delivery of IFN-alpha gene therapy for inhibition of tumor growth located at a distant site. Gene Ther 2001; 8: 400–7.
20 Aoki K, Barker C, Danthinne X, Imperiale MJ, Nabel GJ. Efficient generation of recombinant adenoviral vectors by Cre-lox recombination in vitro. Mol Med 1999; 5: 224–31.
21 Niwa H, Yamamura K, Miyazaki J. Efficient selection for high-expression transfectants with a novel eukaryotic vector. Gene 1991; 108: 193–9.
22 Zhang WW, Koch PE, Roth JA. Detection of wild-type contamination in a recombinant adenoviral preparation by PCR. BioTechniques 1995; 18: 444–7.
23 Yoshida K, Kondoh A, Narumi K, Yoshida T, Aoki K. Extracellular matrix interacts with interferon alpha protein: retention and display of cytotoxicity. Biochem Biophys Res Commun 2008; 376: 299–304.
24 Indraccolo S, Gola E, Rosato A et al. Differential effects of angiostatin, endostatin and interferon-alpha(1) gene transfer on in vivo growth of human breast cancer cells. Gene Ther 2002; 9: 867–78.
25 Hart DN. Dendritic cells: unique leukocyte populations which control the primary immune response. Blood 1997; 90: 3245–87.